2013

Variational Methods in Ice Sheet Modelling

Douglas John Brinkerhoff
The University of Montana

VARIATIONAL METHODS IN ICE SHEET MODELLING

By

DOUGLAS JOHN BRINKERHOFF

Bachelor of Science, University of Montana, Missoula, Montana, 2009

Thesis

presented in partial fulfillment of the requirements
for the degree of

Master of Science
in Computer Science

The University of Montana
Missoula, MT

December 2011

Approved by:

Dr. Steven Sprang, Dean of The Graduate School
Graduate School

Dr. Jesse Johnson, Chair
Department of Computer Science

Dr. Joel Harper
Department of Geosciences

Dr. Mike Rosulek
Department of Computer Science

Brinkerhoff, Douglas, M.S., December 2011 Computer Science

Variational Methods in Ice Sheet Modelling

Chairperson: Dr. Jesse Johnson

A complete simulation of flowing ice requires knowledge of both the fundamental physical principles that govern the stress and energy balances and a framework for assimilating data into a model to help estimate unknown parameters.

Modelling ice is complex, due to the large spatial extent of ice sheets, the multiple scales at which relevant physics operate, and the coupling between heat, stress, and ice rheology. As such, it is usually necessary to make approximations to the equations governing ice flow. At the same time, it is important to have an understanding of the specific assumptions that lead to these approximations. We develop a variational principle for Stokes flow, and neglect certain components in order to obtain the variational principle for the first-order approximation for ice flow. This result is fundamentally the result of assuming bed slopes to be much less than surface slopes, and that vertical resistive stresses are negligible. From a practical standpoint, using automatic differentiation tools on this functional yields a compact model of ice flow that automatically incorporates correct boundary condition. This model is compared to well known benchmark tests. We also present an improved model of ice thermodynamics that operates on enthalpy rather than temperature, avoiding many of the difficulties associated with phase change.

We derive a method for inverting the Blatter-Pattyn ice sheet model in order to solve for the rate of basal sliding. This method uses the adjoint equations of the forward model to obtain the gradient of an error functional, and this is minimized using a quasi-Newton method. These methods are applied to an instrumented streamline of the Greenland ice sheet. We perform numerical experiments on this geometry in order to assess the sensitivity of thermal conditions at the ice sheet bed to perturbations in unknwon parameters. The basal thermal regime is sensitive to changes in geothermal heat flux, with the location of the transition zone between cold and temperate ice being linear sensitive to changes in it. The temperature field of the ice sheet is insensitive to downstream changes in sliding speed due to the short length scales over which longitudinal coupling acts.

Contents

Table of symbols

Symbol	Value	Units	Description
$\mathcal{A}$		J a^{-1}	Ice energy functional
$A(T)$		Pa $a^{\frac{1}{3}}$	Temperature dependent ice hardness
B		m	Bed elevation
$\mathbf{B}$			Arbitrary forcing function
β^2		Pa a m^{-1}	Basal traction coefficient
C_p	2009	J kg^{-1} K^{-1}	Heat capacity of ice
C_w	4181	J kg^{-1} K^{-1}	Heat capacity of liquid water
$\mathcal{D}$		J a^{-1}	Rate of viscous dissipation
ϵ			Small perturbation
$\dot{\epsilon}$		a^{-1}	Strain rate tensor
$\dot{\epsilon}_0$	10^{-30}	a^{-1}	Strain rate regulization
$\dot{\epsilon}^2$		a^{-2}	Second invariant of strain rate tensor
$\mathcal{F}$		J a^{-1}	Rate of frictional dissipation
g	9.81	m s^{-2}	Magnitude of gravitational acceleration
$\mathbf{g}$		m s^{-2}	Gravitational acceleration vector
γ	8.71×10^{-4}	K m^{-1}	Melting point depth dependence
Γ			Model domain boundary
h_0		J	Melting enthalpy at atmospheric pressure
h_i		J	Melting enthalpy at depth
H		J	Enthalpy (inner energy) within ice body
η		Pa a	Ice viscosity
k	6.62×10^7	J a^{-1} K^{-1} m^{-1}	Thermal conductivity of cold ice
κ		m^2 a^{-1}	Diffusivity of temperate and cold ice
L	3.35×10^5	J	Latent heat of fusion
$\mathcal{L}$			Arbitrary differential operator
λ		m a^{-1}	Adjoint velocity
Λ		Pa	Normal force at ice bed
n	3		Dimensionless Glen's flow law parameter
ν	3.5×10^3	kg m^{-1} a^{-1}	Moisture diffusivity in temperate ice
P		Pa	Isotropic pressure
Q		J m^2 a^{-1}	Internal heat generation
q_{geo}	42	mW m^{-2}	Geothermal heat flux
$q_{friction}$		mW m^{-2}	Frictional heat flux
R	8.3	J mol^{-1} K^{-1}	Universal gas constant
ρ	910	kg m^{-3}	Ice density
S		m	Surface elevation
T		K	Temperature
T_{ma}		K	Mean annual surface temperature
$\mathbf{u}$		m a^{-1}	Velocity vector
u		m a^{-1}	Horizontal component of velocity vector
w		m a^{-1}	Vertical component of velocity vector
u_o		m a^{-1}	Observed horizontal surface velocity
x, z		m	Cartesian coordinates
$\dot{\xi}$		a^{-1}	Adjoint strain rate tensor
Ω			Model domain

Introduction

Water ice is a complex fluid, made more complex by the context in which it appears on Earth. A glacier's dynamics are dependent on its geological, meteorological, hydrologic, and geomorphological setting, which are circularly influenced by the ice itself. The complexity of glaciological systems due to interaction with their environment is exacerbated by the constitutive complexities of the ice itself, among which are a strongly non-linear relationship between velocity and stress, an equally strong rheological temperature dependence, and the fact that the internal energy commonly encountered in an ice mass straddles a phase change. These difficulties suggest two important theses regarding ice sheet modelling.

First, we must possess a rigorous understanding of the correctness and applicability of different assumptions about ice sheet physics. In particular, any attempt at modelling ice flow should incorporate physics that can be derived from first principles. Also, the thermomechanical structure of the ice needs to be given sufficient consideration, in particular the transition between ice below the melting point, and ice which is undergoing a phase change.

Second, the modelling of ice sheets needs to be informed by data. There are many poorly constrained parameters that generate leading order effects on a glacier's velocity and temperature fields. Examples of these include geothermal heat flux, the coefficients of static and dynamic friction at the ice base, and so-called enhancement factors, or changes in ice viscosity induced by variations in microscopic ice properties. It is unlikely that these parameters will be measured at a scale such that they will be straightforwardly incorporable into a model.

Simultaneously, there exist data that are widely available, such as surface velocity, temperature, and mass balance. Generally speaking, given only an educated guess about one of these unknown parameters, the likelihood of reproducing the known data is quite low. Thus methods that allow data to inform our estimates unknown parameters, while recognizing physical constraints on those parameters, are sought.

Synoptically, in order for models to represent a plausible approximation of a real ice mass, the model must incorporate a sound theoretical basis while simultaneously acknowledging that which is unknown, using data as available to generate defensible guesses to fill in the gaps.

Objective of thesis

My thesis seeks to further the glaciological community's understanding of variational methods, and how they can be applied to practical problems in glaciology. In practice, this means asking and attempting to answer these questions, among others: Can the flow of glaciers be defined as a minimization problem? What is an efficient way to solve such a problem? Can an analogous framework be used to optimize ice sheet models to currently available datasets? These questions are subservient to the theses stated in the previous section. If we can model ice sheets from the perspective of minimizing energy dissipation, then we will have obtained a more rigorous understanding of the ice physics. Second, if similar methods can be applied to data assimilation, then we will possess a framework for improving our estimation of unknown parameters based on currently available information. In preparing this thesis, my chief aim has been to generate an ice sheet model that implements these methods.

Outline

This thesis consists of four chapters. Chapter 1 is this introduction. Chapters 1 and 2 are a primarily theoretical treatise on variational principles and data assimilation. Chapter 3 documents an application of these methods and is intended to be an independent manuscript. On account of this, some level of redundancy in the information presented therein, particularly theoretical underpinnings, is unavoidable. These works, although related, are independent, and were completed at different times. Therefore, assumptions employed in each may be different. Conclusions are drawn in each chapter individually, although I believe that they do not contradict one another. References are presented collectively at the end of the manuscript.

Chapter 1: A variationally derived ice flow model. This chapter presents the theory and practice of generating of an ice flow model from the perspective of minimizing a functional representing the rate of energy dissipation. It also includes coupling this model to an enthalpy-based formulation of ice thermodynamics. I conduct several experiments which show that the model correctly reproduces several ice sheet model benchmark tests.

Chapter 2: Approximating basal traction using an adjoint-equipped ice sheet model. This chapter presents the theory behind using variational calculus to efficiently calculate the gradient of a data dependent cost functional with respect to many control variables. Written plainly, I show how to make an ice sheet model reproduce measured surface velocities by changing how fast the ice is sliding at its bed. This chapter also includes a treatment of the influence of other unknown model parameters on the assimilation procedure.

Chapter 3: Sensitivity of the frozen-melted basal boundary to perturbations of

basal traction and geothermal heat flux: Isunnguata Sermia, western Greenland. Published under the same title in *Annals of Glaciology* with co-authors T. Meierbachtol, J. Johnson, and J. Harper. In this chapter, I apply the above theory to a section of the Greenland ice sheet which is currently undergoing an extensive fieldwork campaign. I perturb values of geothermal heat flux and basal traction, examine the spatial extent of the propogation of these perturbations, and postulate on fundamental properties of ice sheet physics that explain these extents.

Contribution to glaciological literature

In order to be clear, I will specifically enumerate some key features of this work that contribute to glaciology.

1. I derive a novel way which leverages a variational formulation of ice dynamics to arrive at a common simplification. This method of deriving the simplified equations more transparently elucidates the assumptions that the simplification implies

2. I implement a model which uses a variational principle as the fundamental physical representation of momentum balance, and couple this with automatic symbolic differentiation in order to solve the equations of motion for an ice sheet.

3. I couple this momentum balance to an advanced treatment of ice thermodynamics. While the theory behind the enthalpy method is not new (Aschwanden and Blatter, 2009), its coupling to a higher order momentum balance is.

4. I derive the adjoint method for a higher order ice sheet model with explicit treatment of the vertical dimension. While authors have presented results based on this, there currently exist no publications that sufficiently present the theory such that it could be reproduced (Morlighem et al., 2010).

5. I use the tools listed above to explore the sensitivity of the basal thermal regime of a section of the Greenland ice sheet to a variety of perturbations in order to better understand how stable the ice sheet is in its current configuration

Chapter 1

A variationally derived ice flow model

1.1 Introduction

Modern ice sheet models are usually derived from the incompressible Navier-Stokes equations, coupled with an advection-diffusion equation describing the transfer of heat. Fundamentally, the equations governing ice dynamics are specialized conservation statements for mass, momentum, and energy.

1.1.1 Momentum approximations

Approximations are generally made to the governing equations to make them more tractable. In particular the Navier-Stokes equations are subject to a variety of simplifications which reduce their formidable complexity to problems which are more tractable given modern computing power. The first important simplification made is in neglecting the non-linear inertial terms of the Navier-Stokes equations, yielding the so-called full Stokes model of fluid flow, where all components of the Cauchy stress tensor are retained, and two variables beyond the ice velocity are necessary for closure (pressure and a term representing the force which keeps the ice from falling through the bedrock). This is well justified by the fact that the ratio of inertial to viscous forces in ice is very low, or that the Reynolds number is much less than one.

The first-order approximation, or Blatter-Pattyn equation, is derived by assuming that pressure is a linear function of depth, and by neglecting vertical resistive forces, or the component of the stress tensor that resists horizontal changes in vertical velocity (Pattyn, 2003). From this point, two approximations can be made: The shallow ice approximation, which considers vertical

shear stress as the only important component of the stress tensor (e.g. Huybrechts et al. (1996)), and the shallow shelf approximation, which considers only longitudinal stresses (e.g. MacAyeal et al. (1996)).

These various approximations are the result of asymptotic analyses obtained from non-dimensionalization of the Stokes equations. The Stokes equations are symmetric, and at least positive semi-definite, which is an important property in numerical solution. Although a rigorous mathematical justification for the neglect of certain terms in the first-order approximation has recently been presented (Schoolf and Hindmarsh, 2010), these approximations make no guarantee that they will inherit the amiable numerical properties of the Stokes equations. The fact that these properties exist suggest that there is a more fundamental physical statement which underlies the Stokes equations. This property is the variational principle, which is known to exist for all self-adjoint (that is, symmetric) linear operators. The Stokes equations with non-linear viscosity is obviously not linear, but it is provable (Vainberg, 1964) that this type of nonlinear operator also possesses a variational principle.

The variational principle is a scalar equation which, when minimized, yields the solution corresponding to a physical problem. A common example of a variational principle is the Lagrangian which is taught in elementary classical mechanics to describe the trajectory of a dynamical system. The principle in glaciological applications is analogous. There are several advantages in formulating ice sheet physics in this way. First, the quantities in the variational principle are physically meaningful, each term representing a component of the ice sheet's energy balance. Second, boundary conditions are correctly and consistently incorporated automatically. Third, the variational principle allows constraints to be applied. Finally, by making approximations to the original variational principle for the Stokes equations, we can derive various physics approximations in such a way that they are guaranteed to retain the desirable numerical properties of the full stress balance.

In this work, I implement the variational principle in a model framework, and use it to characterize the fluid dynamics of ice, both through differentiation of the variational principle to form the Euler-Lagrange equations, and as a true minimization problem.

1.1.2 Energy treatment

In addition to the equation for momentum balance, an equally important and oft-neglected component of ice sheet dynamics is the energy balance, or the equation which determines the distribution of heat throughout an ice mass. From a high level perspective, this is just the advection-diffusion equation, which usually presents no especially difficult challenge in terms of its solution. The peculiarities of ice however, make this problem non-trivial.

Foremost amongst the difficulties in modelling ice heat distribution is the obvious constraint that ice, if one wishes to continue calling it such, must remain below a certain melting temperature, which is a function of pressure. The constraint is abrupt, and creates a non-linearity which is not well handled by the gradient based methods which are usually employed for handling more continuous non-linearities (such as the non-linearity in the ice viscosity).

An historic approach to handling this problem has been to sidestep it by clever discretizations of the model domain, and iterative selective application of fluxes into the ice mass. Many of these are neither well documented nor well justified, as most make no constraint on the diffusion of heat when the ice is at the melting point, assuming instead that it is small compared to the heat source terms (e.g. Rutt et al. (2009))

Another approach has been to track the front between ice which is currently at the pressure melting point, and ice which is colder (referred to hereafter as temperate and cold, respectively). The first formulation of an ice model which explicitly tracks the boundary between temperate and cold ice is due to Hutter (1982). In this model, it was assumed that cold ice is modelled using the simple unconstrained heat-equation, while ice at the melting point contains both ice and water, and these both influence the rheological properties of the ice. Greve (2005) updated this model by explicitly considering latent heat in the evolution of the temperate-cold transition front.

This method, while successful, is very complex, and generates additional degrees of freedom in the model necessary for tracking the front between cold and temperate ice. More recently, (Aschwanden and Blatter, 2009) proposed a different method for modelling polythermal ice without the need for front tracking, and without the hard cap of the melting point present in the temperature equation. They show that both water content and temperature are unique functions of specific internal energy, or enthalpy, which can be partitioned into sensible and latent heat. Sensible heat is transported via the heat equation, while latent heat produces water. The phase change is manifested as a jump in the diffusivity of the ice at the cold-temperate transition, and the conversion to temperature and water content is performed after the equation is solved.

This enthalpy formulation is the most appealing of the various methods, as it represents a self-consistent representation of the energy of an ice sheet, and in keeping with the theme of this model, is more fundamental than other representations of energy (such as temperature). In this work, I implement the enthalpy formulation as the model's energy balance, and discuss methods by which this still formidably non-linear problem can be solved.

1.2 Model Physics

1.2.1 A variational principle for momentum balance

A variational principle in the context of fluid mechanics is a functional which describes the way in which the energy in a given system transitions between types. A functional, in turn, is a mapping from a vector space to a scalar field, such as the integration of a function over a geometric domain to yield a scalar. For the particles of classical mechanics, this quantity is known as the Lagrangian, and is defined by the kinetic energy of a system minus its potential energy. The system's governing equations are found by minimizing the Lagrangian. This minimization yields the so-called Euler-Lagrange equations. We can form a similar construction for ice sheet models. For Stokes equations, we neglect inertial terms, so we assume that the system has negligible kinetic energy. This leaves only potential energy and its dissipation into heat to quantify. Minimizing the rate at which this energy conversion occurs yields a solution for the mechanics of an ice sheet. Specifically, an ice sheet loses gravitational potential energy to dissipation as heat.

In what ways can this occur? First, an ice sheet can dissipate energy through viscosity, which is to say that potential energy is converted to heat by the ice's tendency to resist internal deformation. Second, the ice sheet can dissipate potential energy by friction, which is the generation of heat by sliding over a rough bed. These are the only meaningful ways that potential energy can be dissipated in ice. Let us formalize these terms. Much of the following derivation is due to Dukowicz (2011). First, we define an expression for the rate of change of potential energy for some volume of ice:

$$\mathcal{V}(\mathbf{u}) = \int_\Omega \rho \mathbf{g} \cdot \mathbf{u} \, \mathrm{d}\Omega \tag{1.1}$$

where ρ is the density of ice, $\mathbf{g} = (0, g)$ is the gravitational acceleration vector, and $\mathbf{u} = (u, w)$ is the ice velocity vector. Note that this expression is integrated over the entire ice domain, Ω. Next, we define an expression for the rate of heat production through viscous dissipation. The following expression for representing a strain-rate dependent viscosity is due to Bird (1960):

$$\mathcal{D}(\dot{\epsilon}^2) = \int_\Omega \frac{2n}{n+1} \eta(\dot{\epsilon}^2) \dot{\epsilon}^2 \, \mathrm{d}\Omega \,, \tag{1.2}$$

where $\dot{\epsilon}^2$ is the second invariant of the strain rate tensor squared, or written explicitly:

$$\dot{\epsilon}^2 = \frac{\partial u}{\partial x}^2 + \frac{\partial w}{\partial z}^2 + \frac{1}{2}\left[\frac{\partial u}{\partial z} + \frac{\partial w}{\partial x}\right]^2 + \dot{\epsilon}_0 \,, \tag{1.3}$$

where $\dot{\epsilon}_0$ is a small regularization parameter designed to prevent a zero strain rate. To define the

viscosity η, we need a constitutive relationship for ice, which relates stress and strain. Glen's flow law is commonly used and we adopt it here:

$$\eta(\dot{\epsilon}^2) = \frac{A(T)}{2}[\dot{\epsilon}^2]^{\frac{n-1}{2n}} \,. \tag{1.4}$$

$A(T)$ is a temperature dependent rate factor, given by the Arrhenius relation

$$A(T) = \begin{cases} 3.61 \times 10^{-13} \quad \mathrm{e}^{-6.0\times 10^4/RT}, & T \leq 263.15\mathrm{K}, \\ 1.73 \times 10^{3} \quad \mathrm{e}^{-13.9\times 10^4/RT}, & T > 263.15\mathrm{K}, \end{cases} \tag{1.5}$$

and R is the universal gas constant (Paterson and Budd, 1982). n is an exponent that controls the non-linearity of the viscosity, and is commonly taken to be 3 (Glen, 1955). We see that ice viscosity is a nonlinear function of strain rate. We also need an expression for energy dissipation as a result of viscous sliding. For our purposes, we assume that basal sliding velocity and basal shear stress are linearly related by some basal traction coefficient β^2, which is always positive. The following is a general expression for frictional heat generation

$$\mathcal{F}(\mathbf{u}) = \int_{\Gamma_B} \beta^2 \mathbf{u}\cdot\mathbf{u} \, \mathrm{d}\Gamma \,. \tag{1.6}$$

Note that this quantity is integrated over Γ_B, which means that this functional is only considered along the basal boundary. We would not expect frictional heat to be generated anywhere else. Collecting these expressions yields the functional to be minimized to determine the dynamics of the ice mass:

$$\mathcal{A}[\mathbf{u}] = \int_\Omega \left[\frac{2n}{n+1}\eta(\dot{\epsilon}^2)\dot{\epsilon}^2 - \rho\mathbf{g}\cdot\mathbf{u}\right] \mathrm{d}\Omega + \int_{\Gamma_B} \beta^2 \mathbf{u}\cdot\mathbf{u} \, \mathrm{d}\Gamma \,. \tag{1.7}$$

While this statement completely defines the conversion of potential energy into heat within an ice mass, it is not complete, as it fails to account for two constraints which must be imposed on the system to maintain physical plausibility. The first of these constraints is incompressibility of ice, or equivalently, the statement of conservation of mass. This constraint has the form

$$\frac{\partial u}{\partial x} + \frac{\partial w}{\partial z} = 0 \,. \tag{1.8}$$

Also, we must enforce the constraint that there be no velocity normal to the hard bed, or that the ice cannot fall through the bed rock:

$$\mathbf{u}_B \cdot \mathbf{n}_B = 0 \,, \tag{1.9}$$

where $\mathbf{n}$ is the unit normal vector at the bed. One of the appealing aspects of the variational principle is the ability to easily apply these kinds of equality constraints to the system in the form of Lagrange multipliers. Adding these constraints to the system, multiplied by a Lagrange multiplier yields the variational principle for Stokes flow

$$\mathcal{A}[\mathbf{u}, P, \Lambda] = \int_\Omega \left[\frac{2n}{n+1} \eta(\dot{\epsilon}^2) \dot{\epsilon}^2 - \rho \mathbf{g} \cdot \mathbf{u} - P \nabla \cdot \mathbf{u} \right] \mathrm{d}\Omega + \int_{\Gamma_B} \left[\beta^2 \mathbf{u} \cdot \mathbf{u} + \Lambda \mathbf{u} \cdot \mathbf{n} \right] \mathrm{d}\Gamma \,, \tag{1.10}$$

where we have introduced Lagrange multipliers P and Λ. That we chose the symbol P as the Lagrange multiplier for incompressibility is no accident. Lagrange multiplier frequently have a physical interpretation, and in this case, the force which is imposed in order to maintain incompressibility is simply the pressure. Similarly, Λ also has a physical interpretation, which is the force that the earth exerts on the ice mass in order to maintain its position.

In order to verify the correctness of $\mathcal{A}$, we must show that minimizing the functional yields the familiar Stokes equations. Since the functional is positive semi-definite, this is equivalent to finding any extremal point (as there is no maximum). To find the extremal point of a functional, we take its first variation, formally defined as the Gateaux derivative:

$$\delta \mathcal{A}[\mathbf{u}, P, \Lambda] = \lim_{\epsilon \to 0} \frac{\partial}{\partial \epsilon} \mathcal{A}[\mathbf{u} + \epsilon \delta \mathbf{u}, P + \epsilon \delta P, \Lambda + \epsilon \delta \Lambda] \,. \tag{1.11}$$

Setting the first variation equal to zero yields the extremal point. The first variation of the functional after some algebra and an application of integration by parts is

$$\begin{aligned} \delta \mathcal{A}[\vec{u}, P, \Lambda] \quad = \quad & \int_\Omega \left[\nabla \cdot 2\eta \dot{\epsilon} + \rho \mathbf{g} - \nabla P \right] \cdot \delta \mathbf{u} \, \mathrm{d}\Omega + \int_{\Gamma_B} \left[\beta^2 \mathbf{u} + \Lambda \mathbf{n} \right] \cdot \delta \mathbf{u} \, \mathrm{d}\Gamma \\ & + \int_\Omega \left[\nabla \cdot \mathbf{u} \right] \delta P \, \mathrm{d}\Omega \\ & + \int_{\Gamma_B} \left[\mathbf{u} \cdot \mathbf{n} \right] \delta \Lambda \, \mathrm{d}\Gamma \,, \end{aligned} \tag{1.12}$$

where $\dot{\epsilon}$ is the strain rate tensor, given by

$$\dot{\epsilon}_{ij} = \frac{1}{2} \left[\frac{\partial u_i}{\partial x_j} + \frac{\partial u_j}{\partial x_i} \right] . \tag{1.13}$$

For arbitrary variations $\delta \mathbf{u}$, δP, and $\delta \Lambda$, the terms multiplying them must equal zero for $\mathcal{A}$ to be extremal. Setting these coefficients equal to zero yields the following partial differential equations

$$\nabla \cdot 2\eta \dot{\epsilon} + \rho \mathbf{g} - \nabla P = 0 \tag{1.14}$$

with natural boundary condition

$$\left[2\eta\dot{\epsilon} - P\right] \cdot \mathbf{n} = \beta^2 \mathbf{u} + \Lambda \mathbf{n} \tag{1.15}$$

along with

$$\nabla \cdot \mathbf{u} = 0 \tag{1.16}$$

$$\Lambda \cdot \mathbf{n} = 0\,. \tag{1.17}$$

These are the Stokes equations coupled with the statements of incompressability and inpenetrability. Thus a necessary condition for $\mathcal{A}$ to be at an extremal point is that Stokes equations and its constraints must be satisfied. This validates the fact that the variational principle $\mathcal{A}$ is a complete representation of the same ice mechanics captured by Stokes equations, and henceforth, we will operate on the variational principle, rather than on Stokes equations, as it is simpler and more fundamental.

1.2.2 Simplifications to the variational principle

While the above form is complete, it is also quite complex, with three variables to account for (the velocity vector, pressure, and bed normal force). The presence of both constraints makes the solution of the system inefficient, and at present, few models use this full formulation. Simultaneously, the presence of the constraints make $\mathcal{A}$ positive semi-definite rather than positive definite, which implies that the minimization is a saddle point problem since the solutions of P and Λ are not uniquely defined. It may also be the case that certain components of the stress balance are unimportant, and simplifications could be made by neglecting them. These ideas will guide us as we attempt to reduce the Stokes functional to a more easily solved system

Elimination of the Lagrange multipliers

The Lagrange multipliers in $\mathcal{A}$ are included to enforce the constraints that the ice be incompressible (or divergence free) and that the bed be impenetrable. These are enforced by P and Λ respectively. Alternatively, if we drew our solution from a space where these constraints were already satisfied, we would not have to include them. Consider the equation for incompressability

$$\frac{\partial u}{\partial x} + \frac{\partial w}{\partial z} = 0\,. \tag{1.18}$$

We can easily solve for w as a function of u

$$w(u) = \int_B^z \frac{\partial u}{\partial x} \mathrm{d}z'\,. \tag{1.19}$$

Since we've incorporated mass conservation into the definition of w, we can eliminate the Lagrange multiplier P. Similarly, for the impenetrability condition, we can express the vertical velocity at the bed as a function of the horizontal velocity

$$w_B(u_B) = u_B \frac{\partial B}{\partial x}\,, \tag{1.20}$$

where B is the elevation of the basal boundary. If we substitute these into our variational principle, and neglect the now-unnecessary Lagrange multipliers, we get the following:

$$\mathcal{A}[u] = \int_\Omega \left[\frac{2n}{n+1}\eta(\dot\epsilon^2)\dot\epsilon^2 - \rho g w(u)\right] \mathrm{d}\Omega + \int_{\Gamma_B} \beta^2 \left[u^2 + \big(u\frac{\partial B}{\partial x})^2\big)\right] \mathrm{d}\Gamma \tag{1.21}$$

where the definition of the second invariant of the strain rate tensor is now

$$\dot\epsilon^2 = 2\frac{\partial u}{\partial x}^2 + \frac{1}{2}\left[\frac{\partial u}{\partial z} + \frac{\partial w(u)}{\partial x}\right]^2 \tag{1.22}$$

This is now a positive-definite functional, since the saddles induced by the Lagrange multipliers are no longer present. It is also contains integral as well as differential terms. As such, the corresponding Euler-Lagrange equations are now integro-differential equations, which are not soluble by traditional numerical methods. It is also useful in that it has properties which make it more similar to the 1st order approximation of ice physics. It has no pressure or impenetrability, and the vertical velocity is a function of the horizontal velocity. It seems, then a logical place to start in order to find the reduced functional corresponding to the first-order equations.

There are many ways to arrive at the first-order functional, but this derivation elucidates the assumptions made in transitioning from the full stress balance to the first-order balance. One of the features of the first order approximation is that the equations for u and w are uncoupled entirely, which is to say that u has no dependence on w, and the equation for u can be solved, after which w is found by simple quadrature over the ice column. Let that guide our efforts to simplify the unconstrained Stokes functional. Essentially this means that we need to eliminate the vertical integrals which appear in the functional, corresponding to $w(u)$. We note first that $w(u)$ appears in the term for the rate of change of potential energy. We would like a way to write this without having to perform the integration in the vertical. This can be achieved through a few applications of Leibniz's theorem and integration by parts (the operations are given explicitly in Dukowicz (2011), Appendix A). The resulting functional is

$$\mathcal{A}[u] = \int_\Omega \frac{2n}{n+1}\eta(\dot\epsilon^2)\dot\epsilon^2 + \rho g\left[u\frac{\partial S}{\partial x} + u_B\frac{\partial B}{\partial x}\right] \mathrm{d}\Omega + \int_{\Gamma_B} \beta^2\left[u^2 + \left(u\frac{\partial B}{\partial x}\right)^2\right] + \rho g H n_x u \,\mathrm{d}\Gamma\,. \tag{1.23}$$

The gravitational potential term has been written as a function of surface slope and horizontal velocity. The product of the gravitational constant, density, and surface slope is commonly referred to as the driving stress, and its presence, rather than the direct body force $\rho\mathbf{g}$ of the Stokes equations, is another characteristic of the first-order equations. The only other place where vertical quadrature appears is in the definition of the strain rate tensor. A scale analysis indicates the horizontal derivatives of vertical velocity ($\frac{\partial w}{\partial x}$) are second order in the aspect ratio (eg. Schäfer et al. (2008)). These are also known as vertical resistive forces, and generally, they are only of importance in isolated cases, such as grounding line dynamics Morlighem et al. (2010); Nowicki and Wingham (2008). If we neglect them, only differential operators remain.

$$\dot{\epsilon}_{BP}^2 = 2\frac{\partial u}{\partial x}^2 + \frac{1}{2}\left(\frac{\partial u}{\partial z}\right)^2 . \tag{1.24}$$

The final issue is the inclusion of the term u_B in the integral over the ice mass, not just the boundary. This implies a non-local coupling between the boundary and the ice itself, and if discretized, would yield non-sparse stiffness matrices, an undesirable numerical property. The first-order approximations make an explicit assumption that the influence of bed slope is negligible (Pattyn, 2003), yielding the functional

$$\mathcal{A}_{BP}[u] = \int_\Omega \frac{2n}{n+1}\eta(\dot{\epsilon}_{BP}^2)\dot{\epsilon}_{BP}^2 + \rho g u\frac{\partial S}{\partial x}\,\mathrm{d}\Omega + \int_{\Gamma_B}\beta^2 u^2\,\mathrm{d}\Gamma\,. \tag{1.25}$$

This is the functional corresponding to the first-order equations. Before we show that this is true, let us return to the assumptions made in deriving it, of which there are two. First, vertical resistive stresses are negligible, which can be justified by a scale analysis of characteristic dimensions. Second, that bed slopes are small. This assumption has the effect to assuming that the pressure distribution within the ice is hydrostatic, which means that it is a function of ice depth only. This has been justified by various authors (Schoolf and Hindmarsh, 2010; Dukowicz, 2011) by invoking the argument that the dissipation of energy must be a positive definite quantity. It is not clear how that argument extends to deriving the BP in the way presented above.

Now, we have only to take the variation of the functional and show that it is equal to the BP equations. Taking the variation yields

$$\delta\mathcal{A}_{BP}[u] = \int_\Omega \left[\nabla\cdot 2\eta\dot{\epsilon}_{BP} + \rho g\frac{\partial S}{\partial x}\right]\delta u\,\mathrm{d}\Omega + \int_{\Gamma_B} -\beta^2 u\,\mathrm{d}\Gamma\,, \tag{1.26}$$

where

$$\dot{\epsilon}_{BP} = \left(2\frac{\partial u}{\partial x}, \frac{1}{2}\frac{\partial u}{\partial z}\right). \tag{1.27}$$

Setting this equal to zero, we must have that given a small perturbation δu, the functional be

zero. This yields the strong form

$$\nabla \cdot 2\eta \dot{\epsilon}_{BP} + \rho g \frac{\partial S}{\partial x} = 0 \tag{1.28}$$

with boundary condition

$$2\eta \dot{\epsilon}_{BP} \cdot \mathbf{n} = -\beta^2 u \,, \tag{1.29}$$

which correspond exactly to the first-order equations derived by Blatter (1995) and Pattyn (2003).

1.2.3 An enthalpy treatment of the energy balance

Impracticality of a variational formulation

While the use of a variational principle for the momentum balance allowed a convenient framework for the analysis of the model physics, the application of such a construct for the enthalpy equations is less straightforward. The key difference between the two is that the Stokes equations contained no advective component, as we explicitly neglected it. This neglect is justifiable by considering the very low Reynolds number of ice flow. The problem became purely one of momentum-diffusion, so to speak, and was self-adjoint. We can not neglect the non-self-adjoint portion of a heat transport equation, since the Peclet number (a dimensionless quantity relating the relative importance of advection and diffusion) is much greater than one for ice sheets. This means that advection dominates in this system. Since advection is not self-adjoint there is no way to represent it as a variational principle in a non-contrived way.

Still, there does exist a way to derive a functional such that when its first variation is taken, it yields the advection-diffusion equation. The derivation does little to inform us about the actual physics of the system, and the resulting expression contains terms which are of such a magnitude that they cannot be represented by standard floating point numbers (See, for example, Guymon et al. (1970) or Zienkiewicz and Taylor (2000)). Instead, we will content ourselves with the knowledge that this variational principle does exist, and instead operate on its derivative, the PDE formulation of the enthalpy equations. This is no great loss, since these equations are much simpler than the momentum balance, have straightforward boundary conditions, and we do not intend to make any approximations to them.

The enthalpy method

Like any quantity derived from a conservation principle, enthalpy can be modelled by a transport equation:

$$\rho\left(\frac{\partial H}{\partial t} + \mathbf{u}\cdot\nabla H\right) = \rho\nabla\cdot\kappa(H)\nabla H + Q \tag{1.30}$$

where H is enthalpy or total heat, Q is a term representing heat sources, and $\kappa(H)$ is the thermal conductivity of ice. Internal heat generation Q is defined as

$$\frac{2n}{n+1}\eta(\dot{\epsilon}^2)\dot{\epsilon}^2 \tag{1.31}$$

note that this heat production term is the same as the viscous dissipation term from the variational principle for Stokes flow. This makes sense from a conservation of energy standpoint; any potential energy dissipated by viscous dissipation must become heat. This link between heat generation and viscous dissipation is another advantage of casting the momentum balance in a variational form.

The thermal conductivity, $\kappa(H)$ is a function of the enthalpy H, and as such creates a non-linearity in the model. Specifically, κ changes values between cold and temperate ice. We define cold ice such that

$$H < h_i(P) \tag{1.32}$$

where h_i is the enthalpy at which a phase change occurs for a given pressure P

$$h_i(P) = C_w(h_0 - \gamma P) - L \tag{1.33}$$

and C_w is the heat capacity of liquid water, h_0 is the melting enthalpy of ice at atmospheric pressure, γ is the dependence of melting point on pressure, and L is the latent heat of fusion. Temperate ice is any ice which is not cold. With these definitions in hand, we can define the non-linear conductivity as follows:

$$\kappa(H) = \begin{cases} \frac{k}{\rho C_p} & \text{if cold} \\ \frac{\nu}{\rho} & \text{if temperate} \end{cases} \tag{1.34}$$

where k is the thermal conductivity of ice below the pressure melting point, C_p is the heat capacity of ice, and ν is the diffusivity of temperate ice. It is not at all well understood what the value of ν should be. Both Hutter (1982) and Aschwanden and Blatter (2009) have suggested that it be a function of both water content and gravity, but as yet it is unknown what the specific form of such a function should be. In any case, it would have to capture both the diffusion of

liquid water through the ice matrix, as well as the movement of liquid water through macroscopic conduits. In the absence of a good hydrologic model for predicting this value, we take ν to be some constant significantly less than $\frac{k}{C_p}$. Its inclusion is important in order to keep the equation uniformly parabolic. Otherwise, we would have infinite Peclet numbers in temperate ice, and the equations would become hyperbolic. This is undesirable, as it requires a special numerical scheme such as upwinding Zienkiewicz and Taylor (2000).

At the surface boundary, we apply a Dirichlet boundary condition of mean annual surface temperature

$$H_S = C_p T_{ma} \tag{1.35}$$

and at the basal boundary we impose a Neumann condition of inward heat flux, given by

$$\kappa(H)\nabla \cdot H = q_b = q_{geo} + q_{friction} \tag{1.36}$$

where q_{geo} is inward geothermal heat flux, and is assumed known, while $q_{friction}$ is the generation of heat due to sliding at the bed, and is given by the frictional heat dissipation term from the variational principle for momentum balance

$$q_{friction} = \beta^2 \mathbf{u} \cdot \mathbf{u} \tag{1.37}$$

Enthalpy is uniquely related to temperature and water content in the following way

$$T(H,P) = \begin{cases} C_p^{-1}(H - h_i(P)) + T_m(P) & \text{if cold} \\ T_m & \text{if temperate} \end{cases} \tag{1.38}$$

$$\omega(H,P) = \begin{cases} 0 & \text{if cold} \\ \frac{H - h_i(P)}{L} & \text{if temperate} \end{cases} \tag{1.39}$$

where T_m is the pressure melting point for temperature, and ω is the water content of the ice. Various authors have considered a dependence of ice rheology on water content, but we neglect it in this work.

1.3 Solution Methods

1.3.1 Discretization in FEniCS

All subsequent numerical methods are carried out in the finite element package FEniCS (Logg and Wells, 2010). FEniCS is an open source library for the solution of PDEs using the finite

element method. Among its many capabilities, we make use of its capacity to perform automatic symbolic differentiation and its built-in nonlinear solvers.

1.3.2 The finite element method

All PDEs are solved using the finite element (FEM). The FEM is well documented in many books (e.g. Zienkiewicz and Taylor (2000)) and we will only give a brief overview of the concepts here. Consider a linear differential operator $\mathcal{L}$ and some forcing function $\mathbf{B}$. For some function u for which we are trying to find a solution, a linear PDE is defined by the equation

$$\mathcal{L}u = \mathbf{B} \tag{1.40}$$

This is known as the strong form. We can also generate an equivalent weak form by multiplying the equation by an arbitrary (but non-zero) test function ϕ, and integrating over the domain Ω.

$$\int_{\Omega} \big[\mathcal{L}u - \mathbf{B}\big]\phi \mathrm{d}\Omega = 0 \tag{1.41}$$

It is apparent that whenever the weak form is satisfied, the strong form is also satsified, since for non-zero ϕ, $\mathcal{L}$ and $\mathbf{B}$ must vanish for the equality to hold. The fundamental assumption in finite elements is that the solution u can be approximated by a linear combination of piecewise polynomials

$$u = \sum_{i=1}^{n} \phi_i U_i \tag{1.42}$$

These piecewise polynomials must be defined over some division of the finite domain into finite elements (hence the name). The most common procedure is to partition the model domain Ω into a tesselation of disjoint simplices, such that the union of these approximate the domain. A standard assumption is to use these same piecewise polynomials as test functions. This is known as the Galerkin approximation, and if we substitute these into the weak form, we get

$$\sum_{j=1}^{n} \int_{\Omega} \mathcal{L}\phi_j \phi_i \, \mathrm{d}\Omega \, U_j = \int_{\Omega} \mathbf{B}\phi_i \, \mathrm{d}\Omega \tag{1.43}$$

which leads to n equations in n unknowns, these being the coefficients U_j. Neumann boundary conditions can be incorporated into the linear operator through integration by parts, and Dirichlet boundary conditions are incorporated by constructing the test functions such that they satisfy them. This form naturally lends itself to solution as a matrix equation, where the elements of

the matrix $\mathbb{K}$ and vector $\mathbb{F}$ are given by

$$\mathbb{K}_{ij} = \int_\Omega \mathcal{L}\phi_j \phi_i \, \mathrm{d}\Omega \tag{1.44}$$

$$\mathbb{F}_i = \int_\Omega \mathbf{B}\phi_i \mathrm{d}\Omega \tag{1.45}$$

respectively, and the solution coefficients U are found at each nodal point in the mesh by solving the linear system

$$\mathbb{K}U = \mathbb{F} \tag{1.46}$$

1.3.3 A PDE formulation for the Blatter-Pattyn equations

The standard way to solve the momentum balance equations is to discretize the PDE form (equivalent to minimizing the variational principle) and solve them directly. This involves finding the Jacobian of the variational form, which we have already done to verify that this result is, in fact, equivalent to the first order equations from the literature. Although we can obviously do this by hand, it is more concise and consistent to perform all operations on the variational form, so that if we make a change to the variational form, this change is automatically incorporated into the PDE formulation. FEniCS's capacity for automatic differentiation is well suited to this. Everytime we wish to run the model, we simply instruct the software to automatically perform the variation that we did by hand, and discretize those equations as the PDE to be solved. The relationship between the variational form and the finite element method is such that we can consider variations to be test functions, which yields the weak form of the equations suitable for FEM discretization. To review, the discretized equations are

$$\int_\Omega \left[\nabla \cdot 2\eta \dot{\epsilon}_{BP} + \rho g \frac{\partial S}{\partial x} \right] \delta u \, \mathrm{d}\Omega + \int_\Gamma -\beta^2 u \, \delta u \, \mathrm{d}\Gamma = 0 \tag{1.47}$$

1.3.4 A PDE formulation for the Enthalpy equation

Although we know that a variational principle for the enthalpy equations exists, it includes terms of such magnitude that it is not possible for a computer to represent it numerically in a practical way. Because of this issue, in contrast to our automated method for differentiating the BP equations, for the enthalpy equations, we implement the code for the weak form directly. Similarly to the first-order equations, the relationship between the variational form and the finite element method is such that we can consider the arbitrary variation δH to be a test function, which yields the weak form of the enthalpy equation suitable for FEM discretization. This

equation is

$$\int_\Omega \left[\nabla \cdot \kappa \nabla H - \mathbf{u} \cdot \nabla H + Q\right] \delta H \, \mathrm{d}\Omega + \int_\Gamma \left[q_{geo} + q_{friction}\right] \delta H \, \mathrm{d}\Gamma \tag{1.48}$$

1.3.5 A continuous Newton's method for FEM

Since both the momentum balance and enthalpy equations contain non-linear parameters (viscosity and diffusivity, respectively), we need to use a solver which can handle non-linearity. A common method for dealing with non-linearities like these is Newton's method, which is derived from a Taylor series (Nocedal and Wright, 2006). Newton's method can be applied in a variety of ways. In this case, the primary choice is whether to apply it before or after discretization. We choose to apply the method before, so that FEniCS's automatic differentiation tools can be employed. The method works like so: given a PDE in weak form

$$\mathcal{F}(u;\phi) = \int_\Omega (\mathcal{L}(u)u - \mathbf{B})\phi = 0\,, \tag{1.49}$$

we seek the function u, such that the equality holds. Note the correspondence between the notation used here and in the previous section. For this solution procedure, we operate on the operators used in the finite element method. The difference is that now the operator $\mathcal{L}$ is non-linear. Let us expand $\mathcal{F}$ in a Taylor series over an update to the solution Δu

$$\mathcal{F}(u + \Delta u;\phi) \approx \mathcal{F}(u;\phi) + \delta\mathcal{F}(u;\delta u,\phi)\Delta u + \mathcal{O}(\Delta u^2) \tag{1.50}$$

where we have retained only terms of $\mathcal{O}(\Delta u)$. $\delta\mathcal{F}(u)$ is the first variation of $\mathcal{F}(u)$, or more formally the Gateaux derivative. A more common name for this construct is the Jacobian, or $\mathcal{J}(u)$. We seek an update Δu that will make $\mathcal{F}$ equal to zero. If we rearrange the expansion, we find an expression for the update Δu that approximately satisfies this criterion (to $\mathcal{O}(\Delta u)$), given an arbitrary starting point u.

$$\mathcal{J}(u;\delta u,\phi)\Delta u = -\mathcal{F}(u,\phi) \tag{1.51}$$

It is important to note that since we dropped higher order terms, this perturbation will not lead us directly to solution, but it will lead us to a better approximation. This suggests an iterative scheme, where we update u by Δu until the value of $\mathcal{F}$ is sufficiently close to zero. The equation for Δu is still, of course, a continuous PDE. We have to discretize to solve, and we do this by recognizing that the perturbation δu is a trial function, and ϕ, as before, is a test function. u becomes a vector of function values U defined at nodal points. This yields a bilinear

form for $\mathcal{J}(U;\delta U,\phi)$ and a linear form $\mathcal{F}(U,\phi)$, both independent of ΔU. Solving this linear system yields the estimate for the correction vector. The procedure then becomes the following algorithm

Initialize U_n to an initial guess U_0

while $\max(\mathcal{F}(U;\phi)) \geq TOL$ **do**

Solve $\mathcal{J}(U;\delta U,\phi)\Delta U = -\mathcal{F}(U;\phi)$

$U_n += r\Delta U$

end while

where r is a relaxation parameter which is used to control the size of the step taken in the direction of the update. TOL is some small number which defines when the approximate solution is sufficiently close to the actual solution.

1.3.6 Thermomechanical coupling

In order to account for the mutual dependence of velocity and enthalpy, we use a simple Picard iteration (or Fixed-point iteration). This is the most simple of numerical techniques for dealing with non-linearities. The procedure is as follows. Given an initial guess for enthalpy, compute the velocity field. Use this velocity field to compute a new enthalpy. Repeat until neither field changes more than a specified tolerance. The updates between the two fields tend to be small, and this procedure usually converges in less than five iterations.

1.3.7 Time stepping/mesh adaptation

To compute the change in ice geometry at a given time, we use a Crank-Nicholson implicit time stepping scheme (e.g. Zienkiewicz and Taylor (2000)). The continuous equations describing the change in surface elevation over time is

$$\frac{dS}{dt} = \mathbf{u}\cdot\mathbf{n} \approx -u\frac{\partial S}{\partial x} + w \tag{1.52}$$

are discretized using the Crank-Nicholson finite difference, which is a weighted average of the function value at the current time step, and at the future time step

$$\frac{S_{n+1}-S_n}{\Delta t} = \frac{\alpha}{2}\left[-u\frac{\partial S_{n+1}}{\partial x}\right] + \frac{1-\alpha}{2}\left[-u\frac{\partial S_n}{\partial x}\right] + w \tag{1.53}$$

where α is a weighting parameter. Note that the future surface elevation is being calculated in terms of the future surface elevation, so this scheme is implicit for $\alpha > 0$. If $\alpha = 0$, this scheme becomes the simple forward Euler method. If $\alpha = 1$, then it becomes the backwards

L (km)	5	20	80
	Max Mean	Max Mean	Max Mean
Exp. B			
This Work	11.3 10.7	47.4 28.01	96.1 39.76
ISMIP-HOM NFS	10.87 10.54	47.85 27.80	96.43 39.76
Exp. D			
This Work	16.22 16.2	21.43 18.34	98.1 38.0
ISMIP-HOM NFS	12.86 12.85	21.48 18.33	103.77 38.46

Table 1.1: Max and mean values of ISMIP-HOM B and D for the model considered in this paper and the various non-full Stokes models which participated in the benchmark.

Euler scheme. An α of 0.5 generally yields the optimal combination of accuracy and stability. In order to maintain good mesh spacing, S_{n+1} is extruded across the model domain as a function. Then the vertical coordinate of each mesh point N_j is scaled by the following amount

$$z(N_j) = \sigma(N_j)S_{n+1}(N_j) + B(N_j) \tag{1.54}$$

where σ is a rescaled vertical coordinate between zero and one representing the normalized height in the ice column. The surface elevation is constrained such that the ice thickness can never drop below a threshhold H_{min}, in order to avoid inverted mesh elements and the non-physical phenomenon of negative ice thickness.

1.4 Numerical Experiments

In order to verify our solution techniques, we perform the ISMIP-HOM (Pattyn et al., 2008) benchmarks for flowline ice sheet models. These benchmarks are for isothermal models, so only the momentum balance's capacities are tested. In order to verify the energy balance and surface evolution equations, we apply the model to one of the EISMINT II (Huybrechts et al., 1996) benchmark experiments.

1.4.1 ISMIP-HOM B and D

Figures 1.1 through 1.6 give the results of this model's application to the ISMIP-HOM B and D ice sheet model benchmark experiments for example lengthscales $L = \{5, 20, 80\}$. Synoptically, ISMIP-HOM B considers the case of a sinusoidally varying bed with no basal sliding. ISMIP-HOM D considers the case of a uniform surface and bed with sinusoidally varying basal traction coefficient. The experiments are fully outlined in Pattyn et al. (2008). Model statistics compared to the benchmark results are shown in 1.1. This model reproduces the benchmark results accurately for all cases, implying that this model produces results which are consistent with the models that participated in the benchmark.

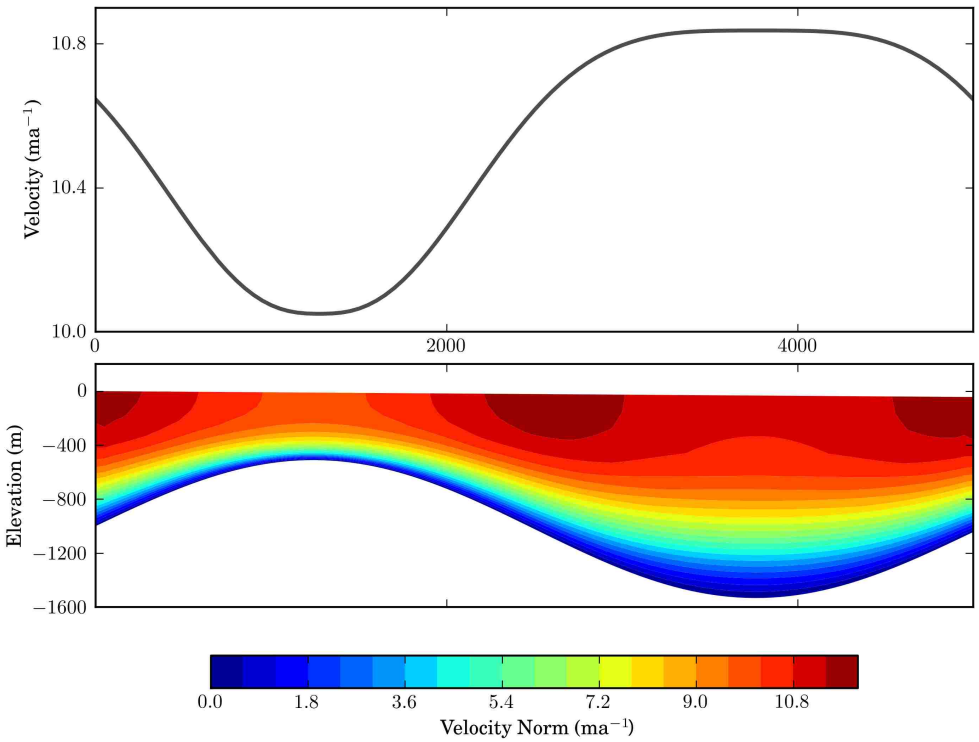

Figure 1.1: Surface horizontal velocity and velocity magnitude for the ISMIP-HOM B benchmark with $L = 5$km

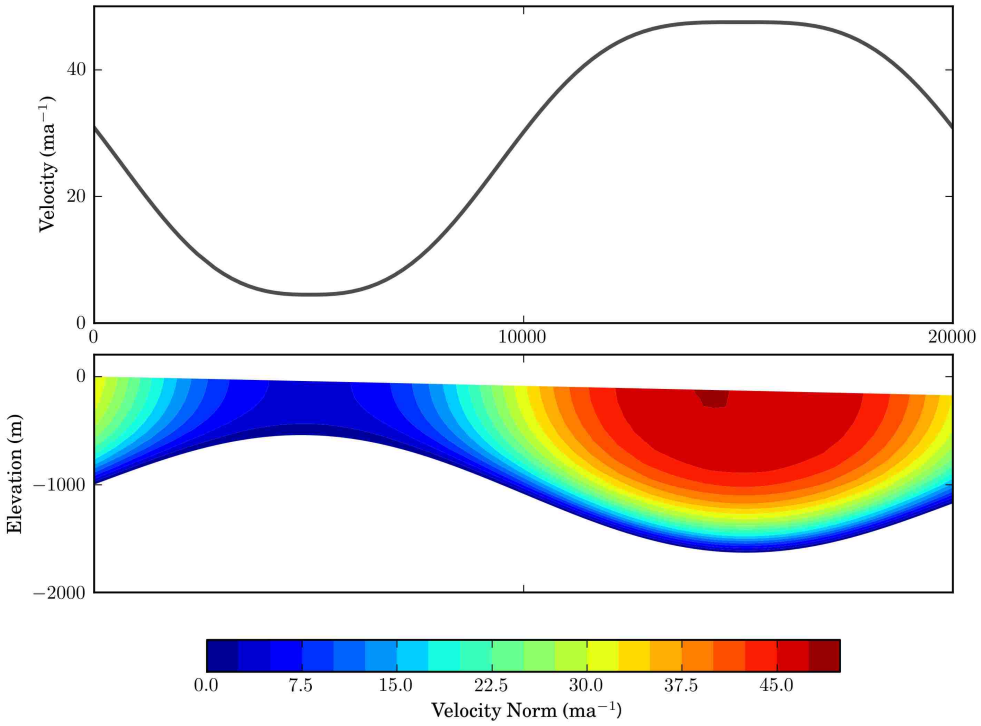

Figure 1.2: Surface horizontal velocity and velocity magnitude for the ISMIP-HOM B benchmark with $L = 20$km

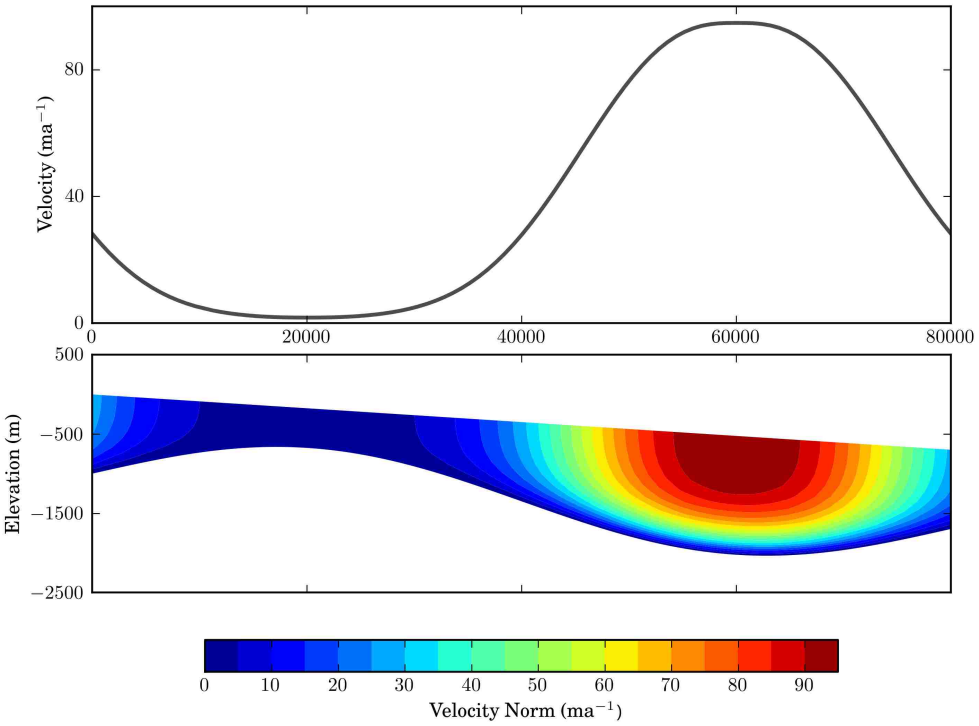

Figure 1.3: Surface horizontal velocity and velocity magnitude for the ISMIP-HOM B benchmark with $L = 80$km

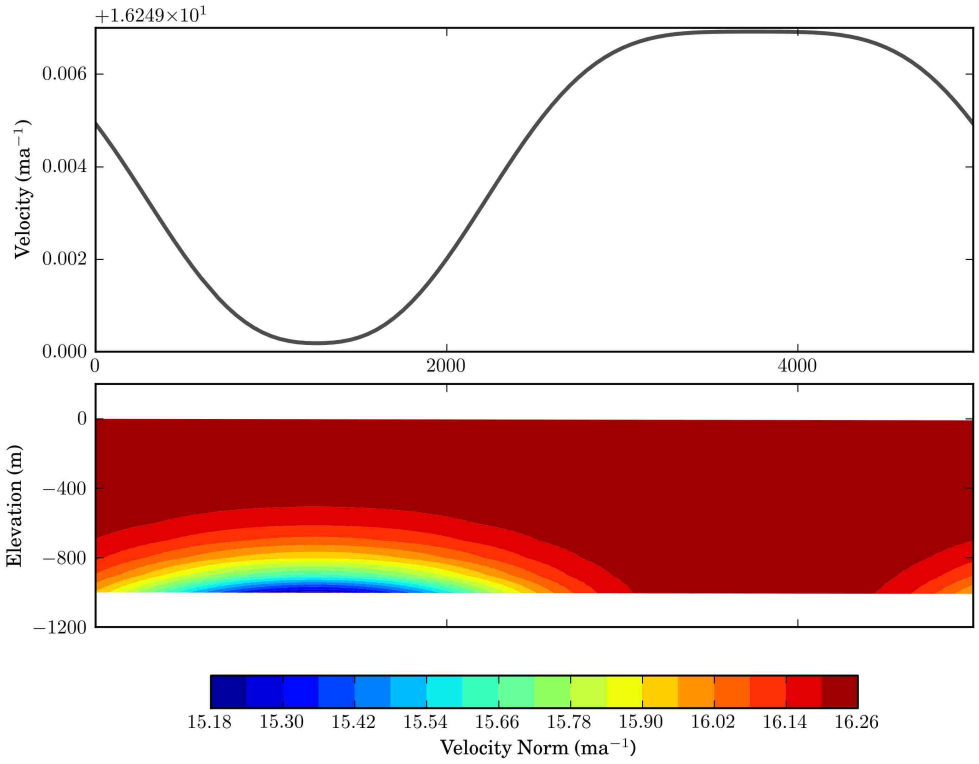

Figure 1.4: Surface horizontal velocity and velocity magnitude for the ISMIP-HOM D benchmark with $L = 5$km

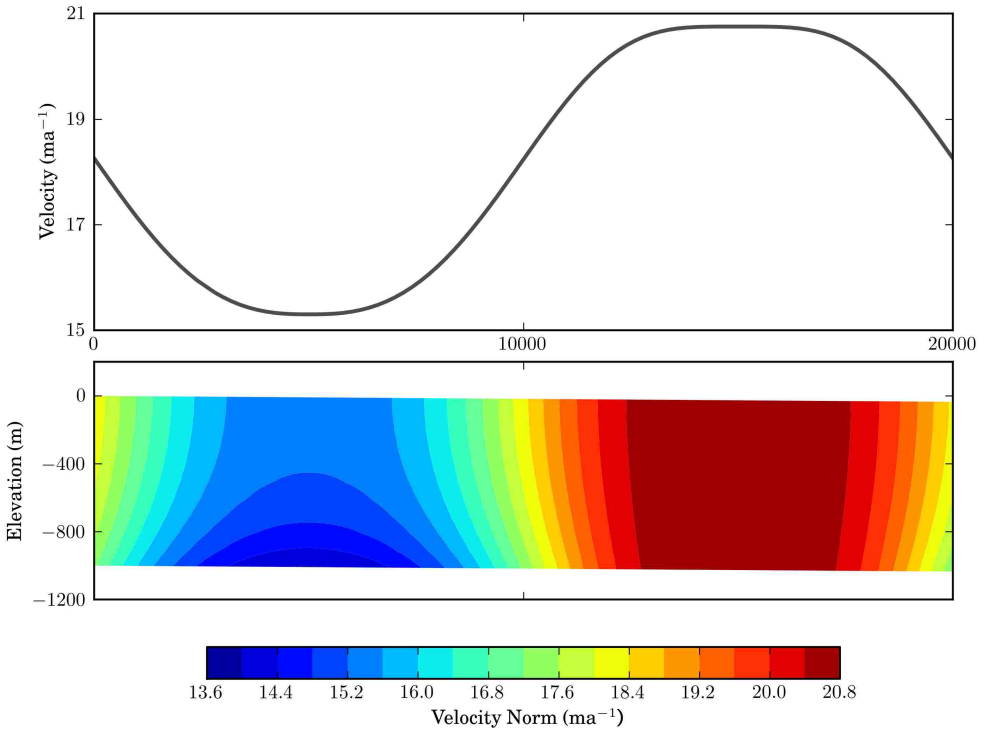

Figure 1.5: Surface horizontal velocity and velocity magnitude for the ISMIP-HOM D benchmark with $L = 20$km

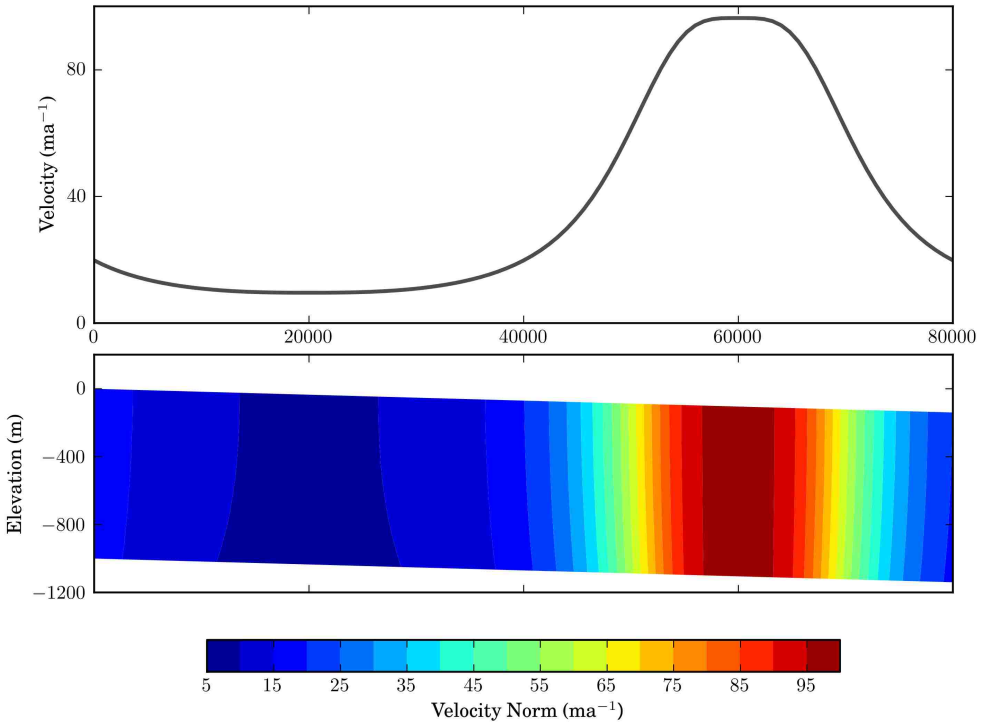

Figure 1.6: Surface horizontal velocity and velocity magnitude for the ISMIP-HOM D benchmark with $L = 80$km

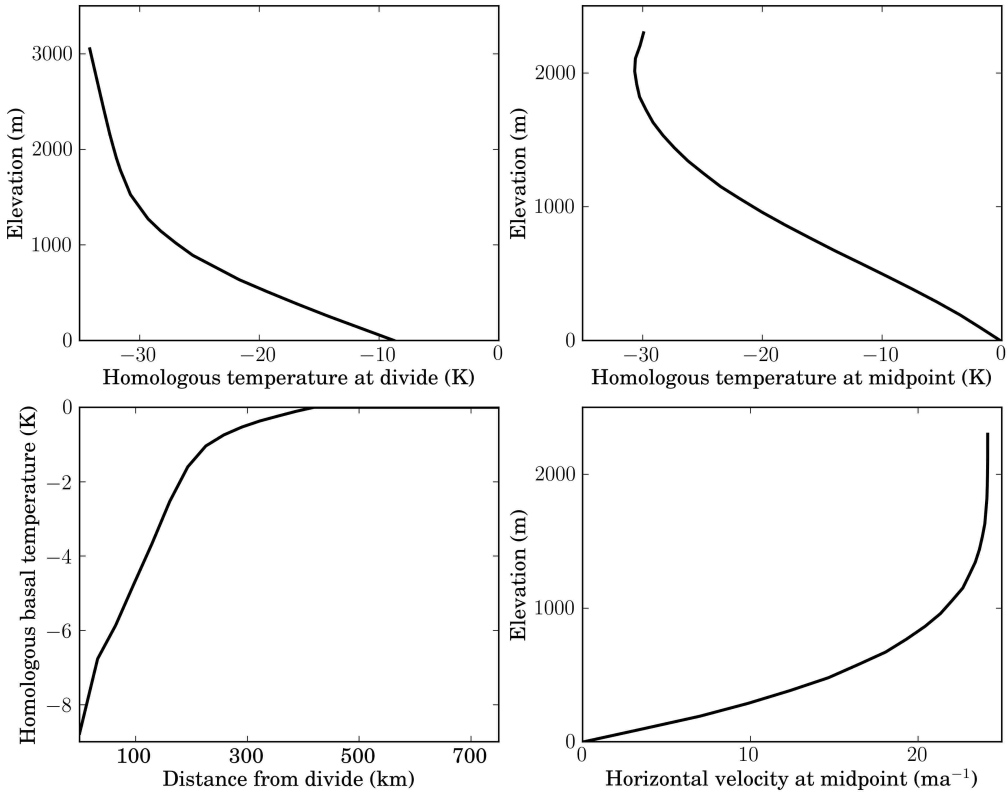

Figure 1.7: Clockwise from top left: 1) Temperature profile at the ice divide, 2)Temperature profile halfway between the divide and terminus, 3) Horizontal velocity halfway between the divide and terminus, 4) Homologous basal temperature for the EISMINT II fixed margin experiment.

1.4.2 EISMINT II

Figures 1.7 and 1.8 gives the results of this model's application to the fixed margin EISMINT II benchmark experiment. Steady state conditions were achieved after approximately 25ka of simulation time. The steady state configuration calculated by this model shows an ice divide elevation approximately 400m lower than the published mean. This difference might be explained either by differences in the momentum balance treatment or differences in the treatment of the free surface. All of the models that participated in the published EISMINT benchmarks used the shallow ice approximation, which neglects longitudinal stresses. Our inclusion of these stresses would affect the model results by producing larger effective strain rates. This would yield a lower ice divide, as ice in the higher order model is more fluid. Alternatively, the Crank-Nicholson scheme may not be capturing non-linearities. The temperature field predicted by the enthalpy model matches the benchmark closely, suggesting that the enthalpy scheme produces results consistent with the models that participated in the intercomparison.

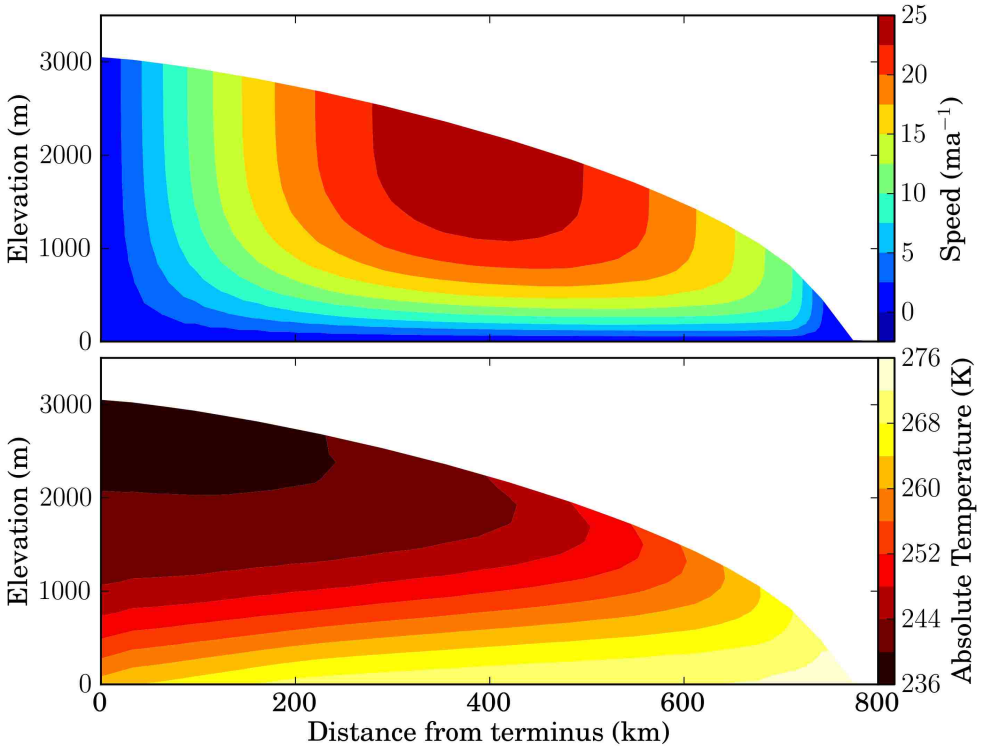

Figure 1.8: Steady state velocity norm and temperature fields for the EISMINT II fixed margin experiment.

1.5 Discussion and Conclusions

Using a variational principle as a starting point for ice sheet modelling provides a robust framework in which to make numerical approximations, explore different solution techniques, and reason about the fundamental physics which are taken into account in an ice sheet model. We have shown how this variational principle can be used to generate consistent approximations to the full momentum balance. Automatic differentiation is a powerful tool in the streamlining of ice sheet modelling, as changes in model physics can be propogated through the solution process solely be changing the variational principle, and allowing automated tools to handle the rest. In this way, we avoid the complex procedure of taking several variations of a complex functional and possible errors in incorporating boundary conditions.

Simultaneously, we have shown an ostensibly better way to handle ice sheet thermodynamics, by posing the energy balance in terms of total heat, rather than only sensible heat flux. This method yields both temperature and water content and avoids the numerically difficult problem of imposing an inequality constraint on the solution of a nonlinear PDE. Although this model is a more complete treatement of the energy balance than standard temperature models, there are yet a number of assumptions in the model that yield unknown parameters. A primary example is the inclusion of a diffusivity in temperate ice, under the justification that movement of moisture content through temperate ice yields a diffusive type heat flux. This could be much improved through the incorporation of an intra-glacial hydrologic model. As of present, no such model exists, although attempts have been made (Flowers et al., 2002). In general, a more accurate description of the movement of heat through the glacier as transported by liquid water should be a non-linear function of water content, gravity, pressure and strain rate.

Here we have developed an implicit-explicit Crank-Nicholson time stepping scheme for solving the surface transport problem. Oscillation-free results have been achieved with this method that match the fixed margin EISMINT model benchmark reasonably well. Despite this success, we are skeptical of our results, especially in the case of a moving margin. More attention needs to be paid to the validity of free surface solution techniques, as the only benchmarked results use techniques which are incompatible with higher order physics.

Chapter 2

Approximating basal traction using an adjoint ice sheet model

2.1 Introduction

Many physical quantities of leading order relevance to glacier and ice sheet flow are either practically impossible to collect, or are point measurements which cannot generally be extrapolated to a broader spatial context. Examples of the former include historic variables such as a detailed record of surface temperature or ice impurity content at depostion. Examples of the latter include basal water pressure, basal temperature, enhancement factors, and geothermal heat flux. A particularly important parameter which as a rule must be estimated is the coefficient of basal traction, which relates basal shear stress to sliding velocity. In many cases sliding makes up nearly all of a glacier's flow (e.g. Weis et al. (1999)), thus any model that wishes to capture the realistic velocity and thermal structure of an ice sheet must incorporate some sort of parameterization of this quantity. The availability of widespread surface velocity data, and the conceptually simple relationship between surface velocity and bed velocity have also made it a popular subject for inverse modelling, and many examples exist of performing forward ice sheet model inversions of varying degrees of complexity in order to determine the basal traction coefficient (MacAyeal, 1993; Goldberg and Sergienko, 2011; Larour et al., 2005; Gudmundsson and Raymond, 2008; Morlighem et al., 2010).

Specific methods for performing the inversion vary. Recently, various authors have had success with using different types of perturbation analyses to solve for unknown parameters (Gudmundsson and Raymond, 2008). Statistical approaches have also been used (Chandler et al., 2006). These models at a basic level make use only of the forward model, which is to say

that they perform their inversions by iterative use of the diagnostic equations of ice sheet motion. This is contrasted to an alternative approach which traditionally has been used to great effect in ice sheet modelling, the use of an adjoint model (MacAyeal, 1993; Goldberg and Sergienko, 2011; Morlighem et al., 2010). The adjoint model is derived in the context of minimizing a functional, with the forward model imposed as a Lagrange multiplier. The methods of variational calculus can then be employed to find the gradient of the functional with respect to a control variable, and standard optimization techniques such as Newton's method can be used. The chief advantage of the use of this method is that the gradient can be found with no more effort than it takes to run the model forward. Contrast this to the finite difference method, where the forward model must be run as many times as there are unknown parameters. While the latter is prohibitively expensive in the case of real applications, the former is trivial once the adjoint equations are known.

The seminal paper of MacAyeal (1993) on the use of control methods in ice sheet modelling applied an incomplete adjoint method to the Shallow-Shelf approximation (SSA), where vertical gradients of horizontal velocity are ignored. More recently, Goldberg and Sergienko (2011) applied the adjoint method to a so-called L1L2 model (Hindmarsh, 2004), which is vertically averaged like the SSA, but employs an iterative correction procedure in order to account for the presence of vertical shear. Their work also represents a jump in analytical complexity, as they find the complete adjoint of their model, as opposed to MacAyeal, who neglected the nonlinearity of ice viscosity.

In this paper, we perform the time honored tradition of inverting surface velocities in order to find the basal traction coefficient. We apply this technique to a flowband of the Greenland ice sheet corresponding to the outlet glacier of Isunnguata Sermia in Western Greenland. We selected this particular site due to it being the subject of a present borehole campaign. Thus in addition to satellite derived surface velocity, model results will eventually be compared to deformation and temperature profiles taken from the boreholes.

2.2 Theory

2.2.1 The forward model.

The forward model in this case is the first-order model given in Chapter 1.

2.2.2 The adjoint model.

In the construction of the adjoint to the forward model, we use basal traction to explain the surface velocity u_S. Specifically, we wish to minimize the following functional which we will call

the objective function

$$\int_{\Gamma_S} \frac{1}{2}(u_o - u)^2 \mathrm{d}\Gamma \tag{2.1}$$

where u_o is some observed surface velocity, or data. Minimizing this functional is obviously very easy, because there is nothing which states that it must obey the forward model. We can incorporate the forward model as a Lagrange multiplier, such that for arbitrary variation in the Lagrange multiplier, the forward model must vanish identically

$$\mathcal{F} = \int_{\Gamma_S} \frac{1}{2}(u_o - u)^2 \mathrm{d}\Gamma + \lambda \left[\int_\Omega \nabla \cdot 2\eta \dot{\epsilon}_{BP} + \rho g \frac{\partial S}{\partial x} \mathrm{d}\Omega + \int_{\Gamma_B} \beta^2 u \mathrm{d}\Gamma \right]. \tag{2.2}$$

If we minimize the above functional with respect to the basal traction field β^2, then we will have found the value of β^2 that minimizes the misfit between observed and modelled surface velocity and still satisfies the model physics. In order to perform this minimization, we proceed as in the previous chapter, by taking the variation of the functional with respect to all three free parameters in the functional, u, λ, and β^2. Note that we treat β^2 as a constant, not as a function of β. The exponent is simply there to remind us that its value must always be positive.

$$\begin{aligned} \delta\mathcal{F} &= \frac{\mathrm{d}}{\mathrm{d}\epsilon} \int_{\Gamma_S} \frac{1}{2}\big[u_o - (u + \epsilon\delta u)\big] \mathrm{d}\Gamma \\ &\quad + (\lambda + \epsilon\delta\lambda) \left[\int_\Omega \nabla \cdot 2\eta \dot{\epsilon}_{BP}(u + \epsilon\delta u) + \rho g \frac{\partial S}{\partial x} \mathrm{d}\Omega + \int_{\Gamma_B} (\beta^2 + \epsilon\delta\beta^2)(u + \epsilon\delta u) \mathrm{d}\Gamma \right] \end{aligned} \tag{2.3}$$

Note that we are ignoring the dependence of the viscosity η on the velocity, which is justified by previous authors (MacAyeal, 1993; Goldberg and Sergienko, 2011) and the fact that the coupling of surface velocity and basal traction is only slightly effected by changes in viscosity. Making this approximation will henceforth be called using the *incomplete* adjoint. We contrast this to using the *complete* adjoint, which involves taking the non-linearities in the viscosity into account when performing these operations. Performing the derivative, and integrating by parts yields the following expression

$$\begin{aligned} \delta\mathcal{F} &= \delta u \left[\int_{\Gamma_S} (u_o - u) \mathrm{d}\Gamma + \int_\Omega \nabla \cdot 2\eta \dot{\xi}_{BP} \, \mathrm{d}\Omega + \int_{\Gamma_B} \beta^2 \lambda \, \mathrm{d}\Gamma \right] \\ &\quad + \delta\lambda \left[\int_\Omega \nabla \cdot 2\eta \dot{\epsilon}_{BP} + \rho g \frac{\partial S}{\partial x} \mathrm{d}\Omega + \int_{\Gamma_B} \beta^2 u \, \mathrm{d}\Gamma \right] \\ &\quad + \delta\beta^2 \left[\int_{\Gamma_B} \lambda \cdot u \, \mathrm{d}\Gamma \right]. \end{aligned} \tag{2.4}$$

The new expression $\dot{\xi}_{BP}$ is the same as $\dot{\epsilon}_{BP}$, except with velocities replaced with the Lagrange multiplier λ

$$\dot{\xi}_{BP} = \left(2\frac{\partial \lambda}{\partial x}, \frac{1}{2}\frac{\partial \lambda}{\partial z} \right). \tag{2.5}$$

For the functional to be stationary given an arbitrary perturbation in the Lagrange multiplier, the forward model must be satisfied. Simultaneously, we have another new PDE which needs to be satisfied for the system to be stationary, the terms multiplying δu. This is known as the adjoint model. Finally, we can calculate the gradient of the functional with respect to β^2 by performing the quadrature of the terms multiplying $\delta\beta^2$. If we take the arbitrary perturbations δu, $\delta\lambda$, and $\delta\beta^2$ as test functions, then the equations are already suitable for discretization by the finite element method, namely they are already in weak form. This is analogous to what happened when we took the variation of the functionals in chapter 2. Still, it is helpful to look at the structure of the equations in strong form. First, we repeat the forward model, writing out the equations in full rather than vector notation:

$$\frac{\partial}{\partial x} 4\eta \frac{\partial u}{\partial x} + \frac{\partial}{\partial z} \eta \frac{\partial u}{\partial z} + \rho g \frac{\partial S}{\partial x} = 0 \text{ on } \Omega \tag{2.6}$$

$$4\eta \frac{\partial u}{\partial x} n_x + \eta \frac{\partial u}{\partial z} n_z = -\beta^2 u \text{ on } \Gamma_B \tag{2.7}$$

$$4\eta \frac{\partial u}{\partial x} n_x + \eta \frac{\partial u}{\partial z} n_z = 0 \text{ on } \Gamma_S \,. \tag{2.8}$$

In addition to homogeneous Dirichlet boundary conditions which are a property of the test functions and do not affect this analysis. Next we write down the strong form of the adjoint equations.

$$\frac{\partial}{\partial x} 4\eta \frac{\partial \lambda}{\partial x} + \frac{\partial}{\partial z} \eta \frac{\partial \lambda}{\partial z} = 0 \text{ on } \Omega \tag{2.9}$$

$$4\eta \frac{\partial \lambda}{\partial x} n_x + \eta \frac{\partial \lambda}{\partial z} n_z = -\beta^2 \lambda \text{ on } \Gamma_B \tag{2.10}$$

$$4\eta \frac{\partial \lambda}{\partial x} n_x + \eta \frac{\partial \lambda}{\partial z} n_z = (u - u_o) \text{ on } \Gamma_S \,. \tag{2.11}$$

The amount of symmetry between the forward and adjoint models is remarkable. The two are identical aside from their forcing functions; the differential operator is the same. This property is known as self-adjointness, and all systems which can be derived from a variational principle are self-adjoint. Note also how the objective function has entered into the adjoint equation. It is a forcing term at the surface, a momentum flux in the parlance of the forward model. Thus the adjoint model can be thought of as modelling the propogation of the objective function's sensitivity through the model domain. Finally, we analyze the form of the gradient function. Solving for the forward and adjoint models means that their contributions to the functional go

to zero and we have

$$\delta\mathcal{F} = \delta\beta^2 \int_{\Gamma_B} \lambda \cdot u \, \mathrm{d}\Gamma \,. \tag{2.12}$$

Thus the change induced in the objective function by a change in β^2 is proportional to the product of basal velocity and the adjoint variable.

2.2.3 Inversion procedure

Inversions of the flowline model (equivalent to minimizing the functional $\mathcal{F}$) are performed using a low memory variant of the Broyden-Fletcher-Goldfarb-Shanno (BFGS) algorithm subject to box constraints (Nocedal and Wright, 2006). BFGS is a quasi-Newton method in the sense that it attempts to minimize the functional by finding the root or zero point of its Jacobian, but unlike a full Newton method, it does not require an explicit determination of the Hessian matrix (See chapter 2 for a description of the multivariate Newton's method). Instead, it computes successive approximations to the full Hessian by taking the finite difference between successive function and gradient evaluations and using them to update the inverse of the Hessian with the Sherman-Morrison formula. For each inversion we select an initial guess and iterate until the gradient of the objective function is very close to zero. In the case of thermomechanically coupled experiments, we developed an initial guess for the thermomechanically coupled solution by first performing the inversion on a fixed temperature run.

2.3 Numerical experiments

2.3.1 ISMIP-HOM D

As we have already shown in chapter 2, our model reproduces the results of the ISMIP-HOM benchmarks quite closely (Pattyn et al., 2008). In order to test the capacity of our inversion technique to reproduce a known basal traction field, we apply it to the 'ice stream' benchmark ISMIP-HOM D, which involves a model domain with a constant ice thickness, uniform surface and bed slope, with a sinusoidally varying basal traction field given by

$$\beta^2 = 1000 + 1000 \sin\left(\frac{2\pi x}{L}\right) \tag{2.13}$$

where L is the length of the model domain.

Figures 2.1 and 2.2 show the results of an inversion on ISMIP-HOM D with domain lengths of 20km and 80km, respectively. We give the convergence profile of the BFGS algorithm, as well as modelled and target surface velocity, and modelled and target values of β^2. The initial guess for this run was a uniform 10^4Pa m a^{-1}, which roughly corresponds to a very slow sliding

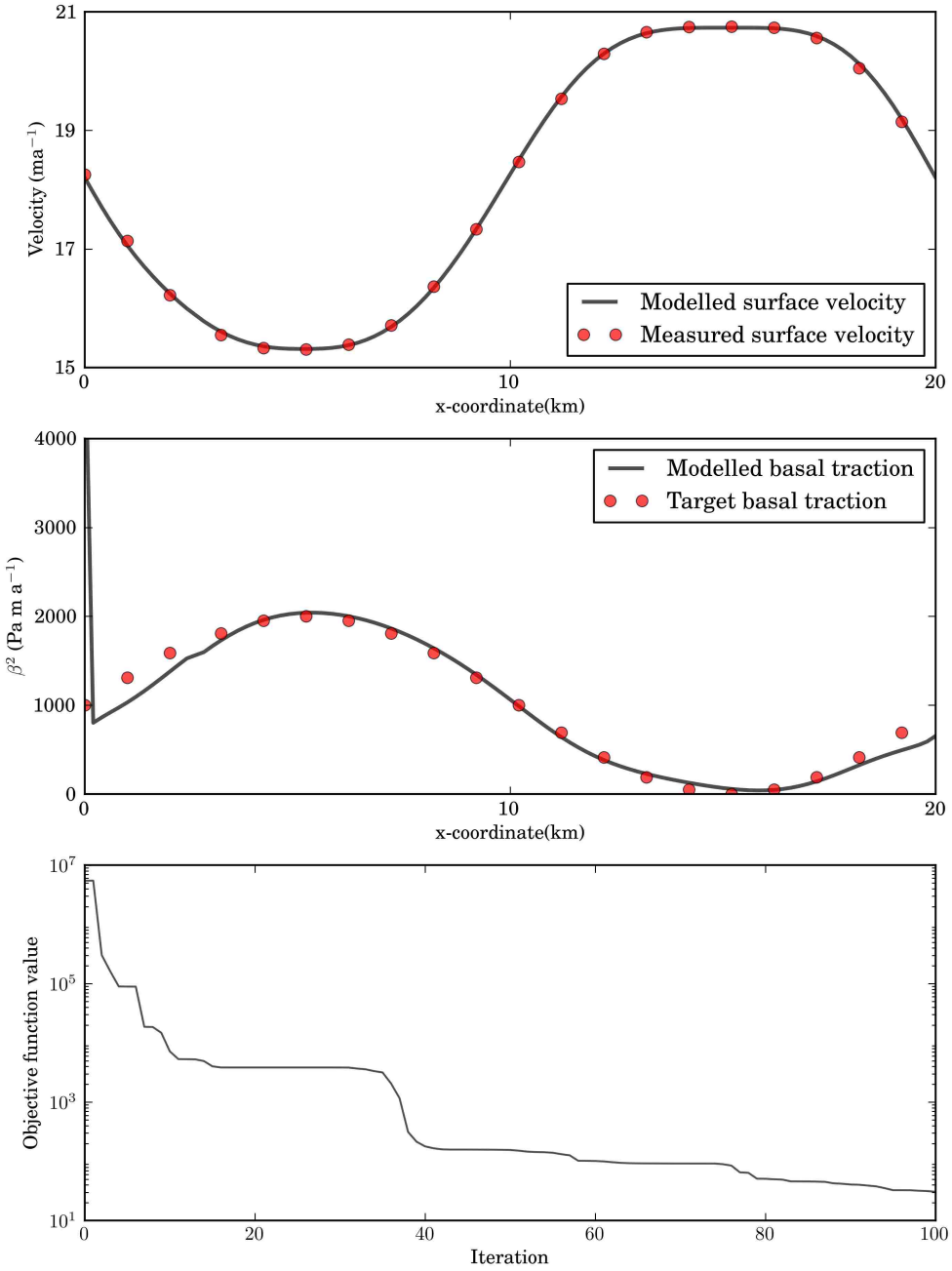

Figure 2.1: Results of ISMIP-HOM D at 20km lengthscale. Top: Observed and modelled surface velocities. Middle: Known and modelled β^2. Bottom: Convergence profile of BFGS algorithm for this inversion

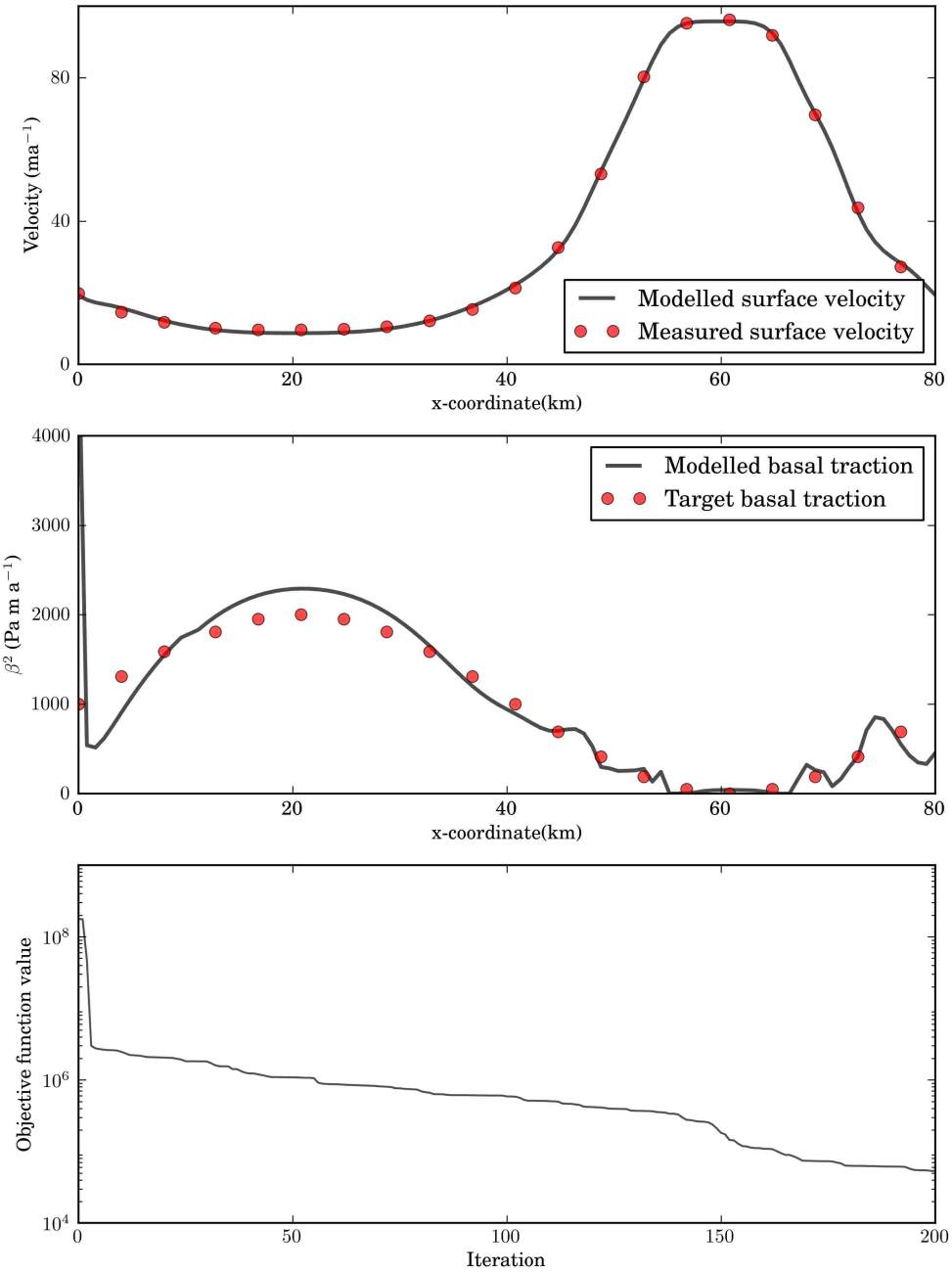

Figure 2.2: Results of ISMIP-HOM D at 80km lengthscale. Top: Observed and modelled surface velocities. Middle: Known and modelled β^2. Bottom: Convergence profile of BFGS algorithm for this inversion

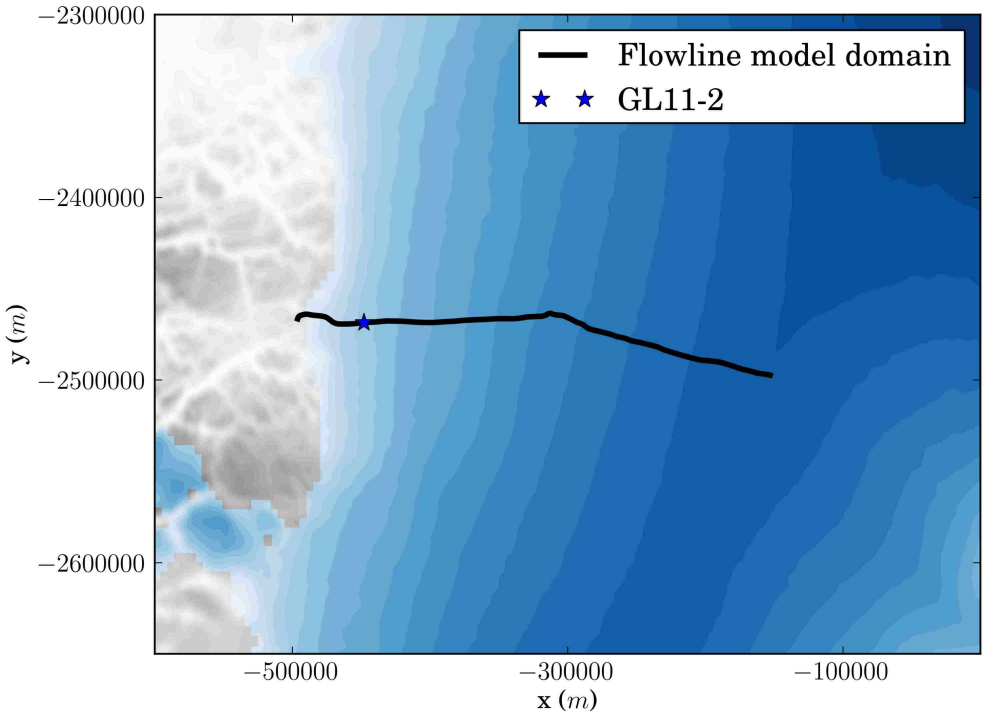

Figure 2.3: Map of flowline extracted from the Greenland ice sheet. Borehole location shown by a blue star.

regime. Convergence is relatively uniform, although stable modes can be seen in the plateaux, which are separated from other plateaux by zones of very fast convergence. The β^2 field for the 20km domain is surprisingly smooth, and comes very close to imitating the sinusoid that it should be. The β^2 field for the 80km domain is less smooth, and exemplifies the fact that solutions to the model inversion are generally non-unique. The surface profiles are very close in both cases.

The β^2 fields, despite being imperfect, are much closer to the target value than those of previous authors. Goldberg and Sergienko (2011) report wildly oscillatory solutions using an incomplete adjoint for a 40km experiment, and a failure of their optimization routine for a length scale of 20km. Also, their results showed a strong dependence of the performance of the incomplete adjoint method on the choice of an initial β^2. Our method shows no such dependence, and tends to converge to the same solution regardless of initial guess.

2.3.2 Isunnguata Sermia

In this section, we apply our inversion techniques to a flowband extracted from the Greenland ice sheet, with a terminus corresponding to the outlet glacier Isunnguata Sermia in western

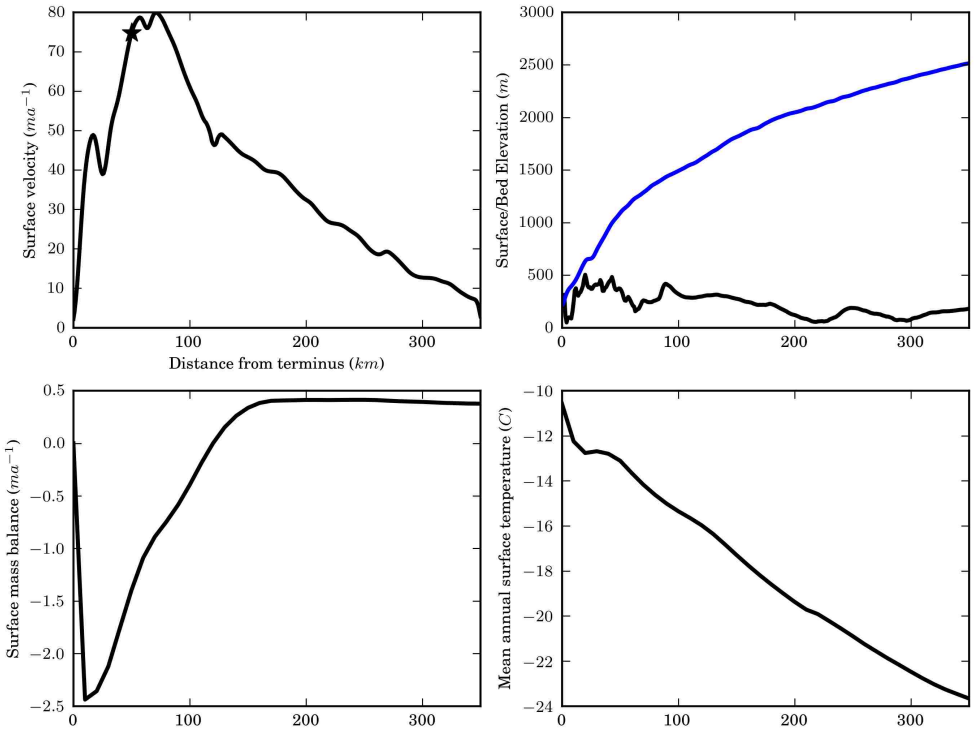

Figure 2.4: Surface velocity, geometry, mass balance, and mean annual surface temperature along the flowline.

Greenland. Figure 2.3 shows a map of the flowband. The flowband was constructed by defining a control point on the glacier surface and following streamlines in the satellite derived surface velocity dataset of Joughin et al. (2010) up to the ice divide and down to the margin. The control point selected was the site of an instrumented borehole, such that borehole data can be applied to the flowband. Surface elevations were extracted from a digital elevation model (DEM) constructed from airborn laser altimetry (Csatho et al. *in press*) and bed elevations from a DEM derived from a combination of surface and airborne radar traces (R. Petterson, *personal comm.*). These data are shown in Figure 2.4.

In this run, we incorporate thermomechanical coupling, such that the viscosity is now dependent on temperature. However, we still use the same assumption of an invariant viscosity. The inversion procedure is indepent of temperature except for in the forward model. The mean annual surface temperature used as an upper boundary condition to the thermomechanical model is extracted from the data-corrected regional climate model of Ettema et al. (2009).

Figures 2.5, 2.6, and 2.7 show the results of this inversion. We give the convergence profile of the BFGS algorithm, as well as modelled and target surface velocity, and modelled values of β^2. Note that the inversion is performed twice. First, a β^2 field is calculated in the absence of thermomechanical coupling. Afterwards, thermomechanical coupling is included, and the inversion is performed again using the results from the first step as an initial guess. The tendency for the BFGS algorithm to take large steps in its line search tends to lead to a divergence in the thermomechanically coupled model, so a good initial guess for this step is crucial.

Convergence is slower for real data, as is to be expected, since the β^2 field and surface velocity fields are more complex. Ultimately, the method converges to a very close representation of the actual surface velocity. Values of β^2 are less smooth in this application than for the ISMIP-HOM experiments, which is a function of the irregularity in bed topography.

2.4 Discussion and Conclusions

Performing the inversion procedure on a known basal traction field is important because it gives us an additional metric by which to judge the quality of the results. It has been shown that inversion procedures of this type are generally ill-posed, in the sense that they have non-unique (and perhaps non-existent) solutions (Goldberg and Sergienko, 2011). Within the bounds of tolerance there are several qualitative patterns which can produce correct surface velocities, and selecting the correct one may be important in terms of model thermodynamics and the comparison of model results to borehole data. One possible solution, as suggested by Morlighem et al. (2010), is to include a Tikhonov regularization term in the objective function, which

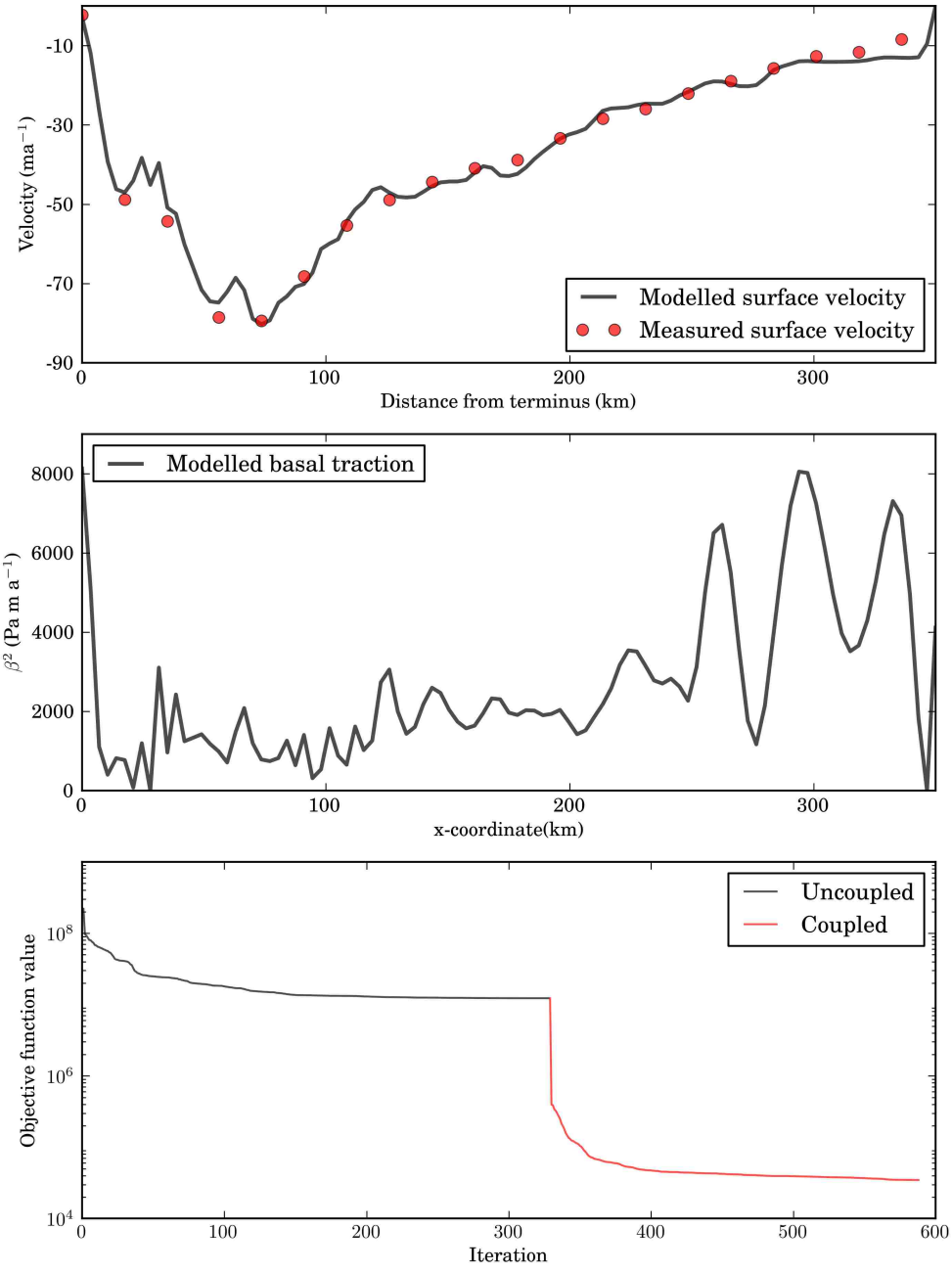

Figure 2.5: Results of an inversion on Isunnguata Sermia, western Greenland. Top: Observed and modelled surface velocities. Middle: modelled β^2. Bottom: Convergence profile for a two-stage BFGS algorithm for this inversion.

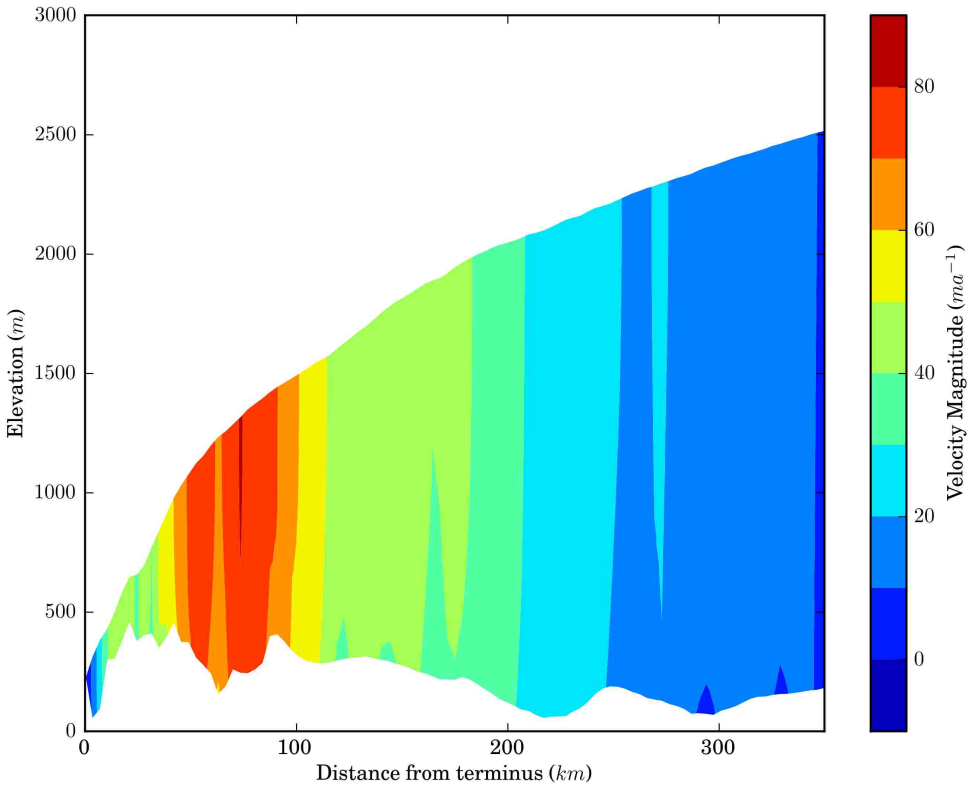

Figure 2.6: Modelled velocity norm field for Isunnguata Sermia, western Greenland after inversion for β^2.

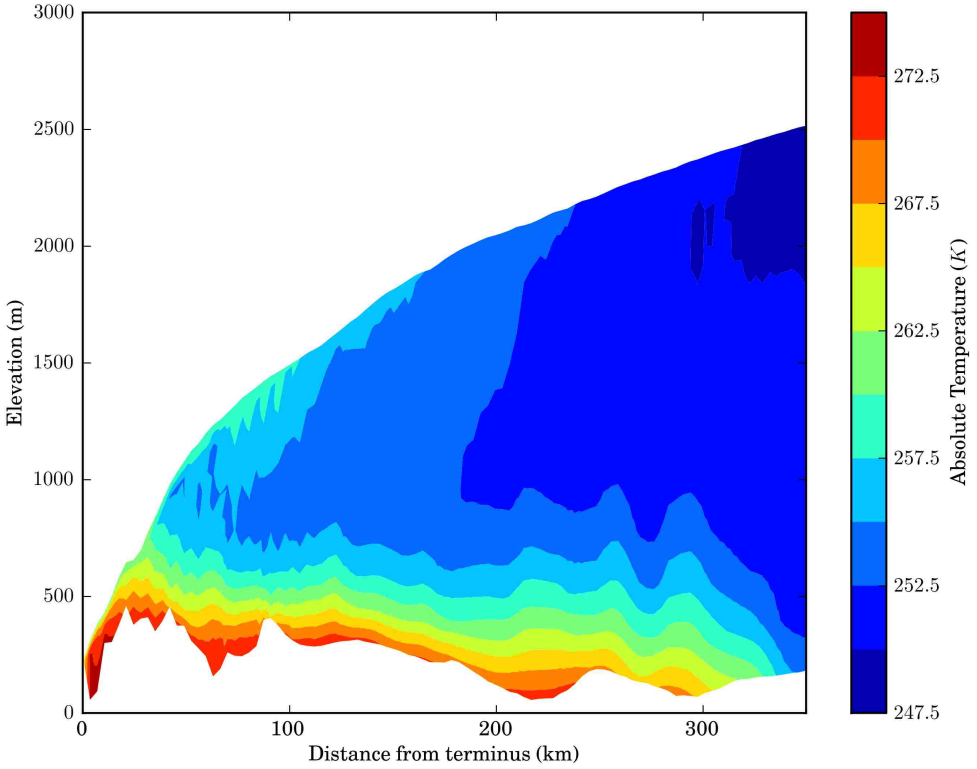

Figure 2.7: Modelled temperature field for Isunnguata Sermia, western Greenland after inversion for β^2.

could essentially penalize the objective function for oscillatory behavior in the β^2 field. This regularization typically takes the form of a weighted squared differential operator, such that the magnitudes of the first or second derivatives of the β^2 field would be added to the objective function. Note that this change would not change the adjoint model, only the calculation of the functional gradient.

It is also worth noting that in the case of inversions on real data sets, there will be inherent flaws in the solutions produced by the inversion procedure due to inconsistencies in the datasets used to generate it. Generally speaking, surface elevation, bed elevation, surface temperature, and surface velocity are all collected at different times, but are nonetheless used as if they were self-consistent and true approximations of the steady state configuration of the ice sheet. This last assumption is not true in most situations. Despite this, the inversion procedure should at least capture some sort of average value.

While the use of the adjoint method in the determination of a basal traction field, other variables could be considered just as easily. Again, the form of the adjoint would not change except for the values of its forcing functions. In this way, an adjoint model could be used to invert for say, an unknown basal topography. Another possibility is using borehole deformation data as a way to determine flow enhancement factors along isochrons. There have been efforts to perform this in a time dependent setting, using an adjoint model to assess the sensitivity of the Greenland ice sheet to perturbations in initial conditions (Heimbach and Bugnion, 2009). With the numerical tools in place, it is now a matter of assembling the relevant datasets to employ these methods.

Chapter 3

Sensitivity of the frozen-melted basal boundary to perturbations of basal traction and geothermal heat flux: Isunnguata Sermia, western Greenland

3.1 Abstract

A full-stress, thermo-mechanically coupled, numerical model is used to explore the interaction between basal thermal conditions and motion of a terrestrially terminating section of the west Greenland ice sheet. The model domain is a two-dimensional flow-line profile extending from the ice divide to the margin. We use data assimilation techniques based on the adjoint model in order to optimize the basal traction field, minimizing the difference between modelled and observed surface velocities. We monitor the sensitivity of the frozen-melted boundary (FMB) to changes in prescribed geothermal heat flux and sliding speed by applying perturbations to each of these parameters. The FMB shows sensitivity to the prescribed geothermal heat flux below an upper threshold where a maximum portion of the bed is already melted. The position of the FMB is insensitive to perturbations applied to the basal traction field. This insensitivity is due to the short distances over which longitudinal stresses act in an ice sheet.

3.2 Introduction

At geologic time scales, high latitude countries in the Northern Hemisphere will likely experience future glaciations. The long term storage of nuclear waste in deep geologic repositories can potentially be impacted by a glaciation via the ice sheet's influence on the subglacial and proglacial groundwater system. It is therefore important to consider subglacial hydrological processes and the role ice sheets play in driving groundwater systems when designing safe storage systems in northern locations. Subglacial hydrological processes become active and recharge the groundwater system only where the bed of an ice sheet is melted. Understanding the spatial pattern of thermal conditions of an ice sheet's bed is therefore an important design criteria for responsible nuclear waste disposal in countries like Sweden, Finland and Canada.

The Greenland Ice Sheet (GrIS) is a present day analog to future ice sheets in Scandinavia and Canada. The thermal state of the bed of GrIS and the accumulation of subglacial water has been investigated by a variety of methods, but remains poorly constrained. Direct observations via drilling show that melted conditions exist near the western margin (Luthi et al., 2002), as well as at a north-central location near the ice sheet divide (Andersen et al., 2004). Conversely, frozen conditions have been noted at point locations spanning the ice sheet from Camp Century near the northwest margin (Weertman, 1968), to the centrally located GRIP core, and the southeast Dye 3 core (Dahl-Jensen et al., 1998). The spatial extent of melted bed conditions as determined by the few point observations has been extended via interpretation of ice penetrating radar. Fahnestock et al. (2001) derived spatially variable basal melt rates exceeding 0.15 ma^{-1} in central GrIS through interpretation of internal radar layering. Using bed reflectivity power as a proxy for basal water content, Oswald and Gogineni (2008) suggested a spatially heterogenous basal water distribution along radar transects of the GrIS.

Spatially comprehensive estimates of basal conditions are offered by ice sheet model output. Greve and Hutter (1995) investigated the sensitivity of the basal temperature field on the Greenland ice sheet to variations in a uniform geothermal heat flux. Their results suggested that, while increasing heat flux caused an inland migration of temperate basal conditions, the interior remained frozen, even under the highest heat flux scenario (54.6 mWm^{-2}). This was complemented by a follow-up investigation of the basal temperature field by matching geothermal heat flux to point observations, which implied that the majority of the ice sheet bed was at the pressure melting point (Greve, 2005). In addition to geothermal heat flux, the sensitivity of GrIS basal conditions to changes in surface temperatures and mass balance was investigated by Huybrechts et al. (1996), who found that basal conditions show a pronounced sensitivity to steady state changes to temperature and mass balance; *e.g.* a 10°C drop in surface temperature resulted in a freezing of the majority of the ice sheet bed, however, the drop in surface mass

Parameter	Symbol	Value
Gravitational acceleration	$\mathbf{g}$	9.81 m/s^2
Thermal conductivity of ice	k_i	2.1 W/m K
Density of ice	ρ	911 kg/m^3
Heat capacity of ice	c_p	2093 J $kg^{-1}K^{-1}$
Latent heat of fusion of ice	L	3.35×10^5 J kg^{-1}
Triple point of water	T_0	273.15 K
Pressure dependence of melting	b	-9.8×10^{-8} K/Pa
Universal gas constant	R	8.314 J/mol K
Seconds per year	-	31556926 s a^{-1}
Glen's flow law exponent	n	3
Viscosity regularization	$\dot{\epsilon}$	10^{-30} Pa s

Table 3.1: Parameters and physical constants used in the model.

balance associated with a 10°C lowering of surface temperature resulted in temperate conditions over nearly 60 percent of the bed. Transient simulations over the last two glacial cycles showed most of GrIS exhibits frozen conditions at the bed at some point in time. While the models employed by both Greve and Huybrechts were three-dimensional, both were mechanically limited to the shallow ice approximation.

In summary, previous studies suggest a spatially distinct frozen-melted boundary (FMB). The location of the FMB at the bed is the result of a balance between heat sources concentrated near the bed (frictional heat from sliding, geothermal heat flux, and strain heating), and the introduction of colder ice through diffusive and advective processes. In the present study, we investigate the sensitivity of the FMB not only to geothermal heat flux, but also to changes in cold ice advection resulting from ice motion, including basal sliding. Sensitivity is investigated with a steady-state, thermomechanically coupled, two-dimensional flow line model which solves the full-stress equations (a vertically explicit solution that includes membrane stresses). We apply this model to a profile of Isunnguata Sermia, a terrestrially terminating glacier in western GrIS. The model is brought into agreement with observation by using adjoint methods for evaluating gradients of an objective function. Motivation for selecting a terrestrially terminating glacier stems from the fact that the majority of the GrIS is land terminating, and such a profile removes additional physical complexities relating to marine-terminating ice. Using the steady state glacier geometry and surface velocity field, we examine the interactions of heat sources that dictate the stability of the FMB under different assumptions about geothermal heat flux and the basal traction fields.

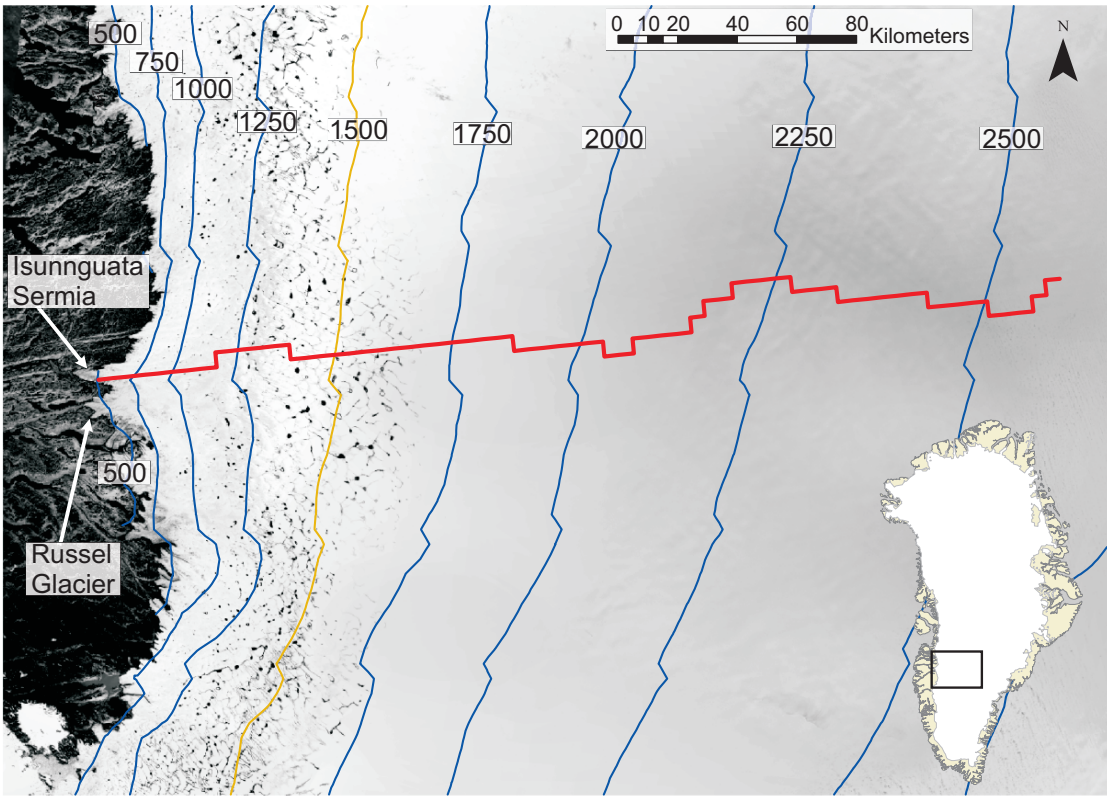

Figure 3.1: Study site displaying model profile (red line) from the ice sheet divide through Isunnguata Sermia to the western margin. Surface elevation contours (blue lines) are given in meters above sea level, and interpolated from Bamber et al(2001). Yellow contour at 1500 m a.s.l. represents the approximate equilibrium line altitude (ELA) according to van de Wal et al. (2008).

3.3 Methods

3.3.1 Field equations

Our model is built upon the continuum mechanical formulation of the laws of conservation of mass, momentum, and energy for an incompressible fluid. These are, respectively;

$$\nabla \cdot \mathbf{u} = 0, \tag{3.1}$$

$$\rho \frac{d\mathbf{u}}{dt} = \nabla \cdot \sigma + \rho \mathbf{g}, \tag{3.2}$$

$$\frac{d\theta}{dt} = \frac{1}{\rho c_p} \nabla \cdot k_i \nabla \theta - \mathbf{u} \cdot \nabla \theta + \frac{\Phi}{\rho c_p}. \tag{3.3}$$

$\mathbf{u}$ represents the velocity vector, σ the stress tensor, θ the temperature, and Φ sources of heat generation in the ice. Physical constants c_p, k_i, ρ, and $\mathbf{g}$ are defined in Table 3.1. Analysis is restricted to the xz plane, or the vertical profile, making $\nabla = \frac{\partial}{\partial x}\hat{i} + \frac{\partial}{\partial z}\hat{k}$, where $\hat{i}$ and $\hat{k}$ are unit vectors in the x and z directions, respectively.

Conservation of momentum and mass

The constitutive relation for ice takes the form

$$\tau_{ij} = 2\eta \dot{\epsilon}_{ij}, \tag{3.4}$$

τ_{ij} is the ij element of the deviatoric stress tensor, which is defined by $\tau_{ij} = \sigma_{ij} - p\delta_{ij}$, and δ_{ij} is the Kronecker delta function. Isotropic pressure is defined as $p = -\frac{1}{3}\sum_i \sigma_{ii}$. $\dot{\epsilon}_{ij}$ represents the corresponding element of the strain rate tensor, and η the viscosity. The strain rate tensor is given by, and related to velocity gradients as follows

$$\dot{\epsilon}_{ij} = \frac{1}{2}\left(\frac{\partial u_i}{\partial x_j} + \frac{\partial u_j}{\partial x_i}\right). \tag{3.5}$$

A non-Newtonian rheology is used for ice

$$\eta = \frac{1}{2} A(\theta^*)^{-1/n} (\dot{\epsilon}_{\Pi} + \dot{\epsilon}_0)^{(1-n)/n}, \tag{3.6}$$

with $\dot{\epsilon}_{\Pi}^2 = \frac{1}{2}\Sigma_{ij}\dot{\epsilon}_{ij}\dot{\epsilon}_{ij}$, or the second invariant of the strain rate tensor, and $\dot{\epsilon}_0$ is a regularization parameter introduced to avoid a singularity at zero strain rate. Glen's flow law (Paterson, 1994)

gives n=3. $A(\theta^*)$ is the flow law rate factor, given by Paterson and Budd (1982).

$$A(\theta^*) = \begin{cases} 3.61 \times 10^{-13} \quad \mathrm{e}^{-6.0\times10^4/R\theta^*}, & \theta^* \leq 263.15\mathrm{K}, \\ 1.73 \times 10^{3} \quad \mathrm{e}^{-13.9\times10^4/R\theta^*}, & \theta^* > 263.15\mathrm{K}, \end{cases} \tag{3.7}$$

where θ^* is the homologous temperature, defined by $\theta^* = \theta + bp$, and R the universal gas constant.

Under the assumption of steady state, the velocity of the ice is then determined from Stoke's flow confined to the xz plane

$$\nabla \cdot \sigma = \rho \mathbf{g}, \tag{3.8}$$

and the conservation of mass $\nabla \cdot \mathbf{u} = 0$.

Conservation of energy

Φ, the term in Equation 3.3 which represents internal heat generation, is computed as

$$\Phi = 2\eta\dot{\epsilon}_{\mathrm{II}}^2. \tag{3.9}$$

Under the assumption of steady state, and uniform thermal conductivity, the temperature of the ice is given by the following equation:

$$0 = \frac{k_i}{\rho c_p}\nabla^2\theta - \mathbf{u}\cdot\nabla\theta + \frac{2\eta\dot{\epsilon}_{\mathrm{II}}^2}{\rho C_p}. \tag{3.10}$$

3.3.2 Boundary Conditions

Boundary conditions are applied to three distinct regions on the boundary of Isunnguata Sermia; (1) the surface, (2) the bed, and (3) a vertical boundary at the ice divide.

Conservation of Momentum and Mass Boundary Conditions

The surface of the glacier upholds the neutral or stress free boundary condition

$$\sigma\hat{\mathbf{n}} = 0, \tag{3.11}$$

where $\hat{\mathbf{n}}$ is the outward normal unit vector.

The bed of the glacier is subjected to a Weertman style sliding law, where basal velocity and shear stress are related as

$$\tau_{\mathbf{b}} = \beta^2\mathbf{u}\cdot\hat{\mathbf{t}} \tag{3.12}$$

where β^2 is a positive scalar, spatially variable parameter representing the magnitude of frictional forces at the bed, and $\tau_{\mathbf{b}}$ is given by

$$\tau_{\mathbf{b}} = \sigma \hat{\mathbf{n}} \tag{3.13}$$

evaluated at the base of the glacier. We constrain the sliding velocity to be tangential to the bed, that is $\mathbf{u} \cdot \hat{\mathbf{n}} = 0$.

The vertical boundary at the divide, is subject to a symmetry boundary condition,

$$\hat{\mathbf{n}} \cdot \mathbf{u} = 0 \tag{3.14}$$

$$\sigma \cdot \hat{\mathbf{t}} = 0, \tag{3.15}$$

where $\hat{\mathbf{t}}$ is the unit vector tangent to the divide.

Conservation of Energy Boundary Conditions

The bed of the glacier is subject to an inward heat flux given by

$$Q = q_g + q_f - q_l \tag{3.16}$$

where q_g is the geothermal heat flux, q_f is heating due to sliding friction, and q_l is latent heat associated with the melting of ice. q_g is a prescribed value of 42mW/m^2, unless otherwise stated. Frictional heat is calculated as

$$q_f = \mathbf{u} \cdot \tau_{\mathbf{b}}. \tag{3.17}$$

Latent heat is given by

$$q_l = \begin{cases} q_f + q_g + k_i \frac{\partial \theta}{\partial z}, & \theta^* \geq 273.15 \\ 0, & \theta^* < 273.15 \end{cases} \tag{3.18}$$

This heat interacts with the ice via the Neumann boundary condition

$$-\hat{\mathbf{n}} \cdot k_i \nabla \theta = Q. \tag{3.19}$$

Note that the inclusion of the latent heat term serves as a temperature constraint on the ice by counteracting the inward flux from geothermal heat and frictional heat when the basal ice is at the pressure melting point.

The surface temperature of the glacier is inferred from the dataset of Ettema et al. (2009), and is imposed as a Dirichlet boundary condition. The vertical boundary at the divide is thermally

Quantity	Value
Mesh Elements	632
Degrees of Freedom	4686
Element Type	Lagrange Quadratic
Initial Damping Factor	1×10^{-4}
Minimum Damping Factor	1×10^{-8}
Criterion for Convergence	$<1\times10^{-6}$

Table 3.2: Quantities of importance for model numerics.

insulated such that $\hat{\mathbf{n}} \cdot [-k_i \nabla\theta] = 0$.

3.3.3 Model Domain

The geometry for the model domain was derived from surface elevation and thickness data of Bamber et al. (2001). Since the model used here considers only a vertical profile, we selected a streamline from the surface velocity data presented in Joughin et al. (2010). We employed cubic splines to interpolate the glacier geometry between data points, which were spaced at 5 kilometers.

Due to the discrete nature of the original dataset, the profile surface contained numerous artifacts, manifested as irregularities in slope. In order to produce a more reasonable surface, we implemented a free-surface evolution scheme, and allowed the model geometry to relax for 50 years. The high driving stresses associated with the slope irregularities quickly diffused, yielding a surface free from the original artifacts, and still consistent with the data and model physics.

3.3.4 Numerical Considerations

The model uses the finite element method to solve the field equations subject to the boundary conditions. Lagrange quadratic elements are used (Hughes, 2000), allowing second derivatives of the velocity to be computed accurately. The non-linearity resulting from the viscosity (Equation 3.6) is resolved by using the modified Newton's method iterative solver (Deuflhard, 1974). The resulting linear systems were solved with UMFPACK (Davis, 2004). Model specific parameters are summarized in Table 3.2. All numerical work was carried out in the *Comsol Multiphysics* modeling environment, a commercial package for finite element analysis of general partial differential equations.

3.3.5 Modeling assumptions

Several assumptions were made in the development of this model, and results must be understood with these in mind. These assumptions are as follows:

1. The data sets used in the generation of the model domain geometry are sufficiently accurate, and the surface smoothing used to reduce artifacts does not introduce additional errors larger than those resulting from artefacts in surface geometry.

2. Stresses acting transverse to the dominant flow direction are small. This is necessary due to the effect that these stresses, and associated strains, have on the rheologic properties of the ice. Given the profile's location at the center of the ice catchment, and the uniform width of the streaming feature, this assumption is likely valid.

3. The steady steady state solution generated by the data assimilation process is a reasonable representation of a long term configuration for the model domain. This assumes that the modeled region of the GrIS was not in a transient state at the time that data was collected.

4. A constant geothermal heat flux is an appropriate parameterization of the real phenomenon across the modelled domain. This is to say that given the spatial scale under consideration, variability in geothermal heat flux is either of a sufficiently low resolution to be considered in an average sense, or of a sufficiently large scale that it is essentially constant.

5. Steady state solutions which include the data assimilation process are sufficient for probing the sensitivities of the system with respect to changes in the basal boundary. A more complete treatment would entail the evolution of the free surface to determine the ultimate outcome of the perturbation, but that is beyond the scope of this work.

3.3.6 Data assimilation and model initialization

When modeling ice dynamics, there are two issues that must be addressed before numerical experiments can be conducted. First, fields which have not been directly measured but are significant in computing flow must be estimated. For instance, the internal distribution of temperatures are critical to ice dynamics, but are at best known at a few boreholes. We will refer to this process as model initialization. Secondly, the initialized model should be in agreement with measurements that are available. We refer to this as data assimilation.

Our strategy in this paper will be to use steady state solutions to conservation equations to initialize the model subject to the constrains introduced by the data assimilation process. This is not a new idea, MacAyeal (1993) introduced control methods in the context of ice sheet modeling. Here, we extend the concepts to solutions which incorporate the full flowline stress balance.

For data assimilation, we use the adjoint of the linear operator to compute derivatives of an objective function, and use those slopes to minimize the function. We have defined an objective

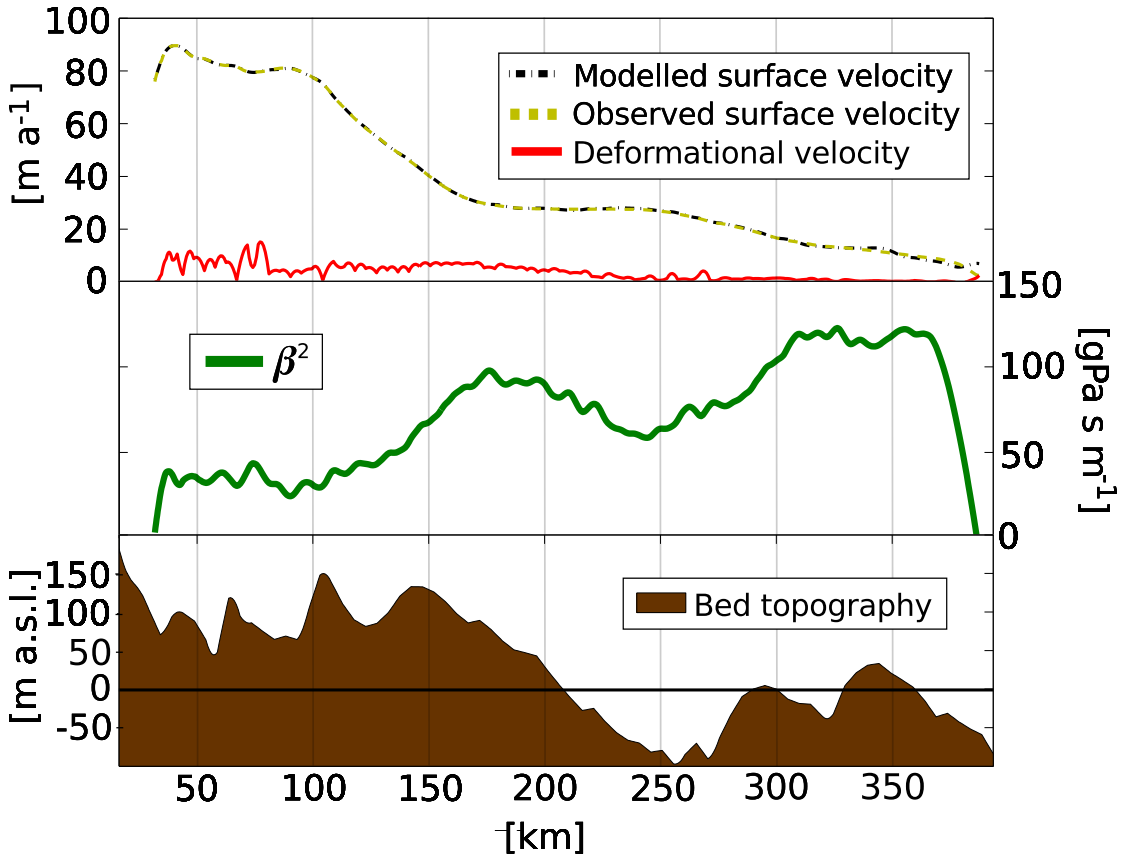

Figure 3.2: Top panel shows the modelled and observed velocity, as well as the portion of the modelled velocity accounted for by internal deformation. The middle panel shows the β^2 field derived from the data assimilation procedure. The lowest panel shows the topography underlying the modelled ice profile.

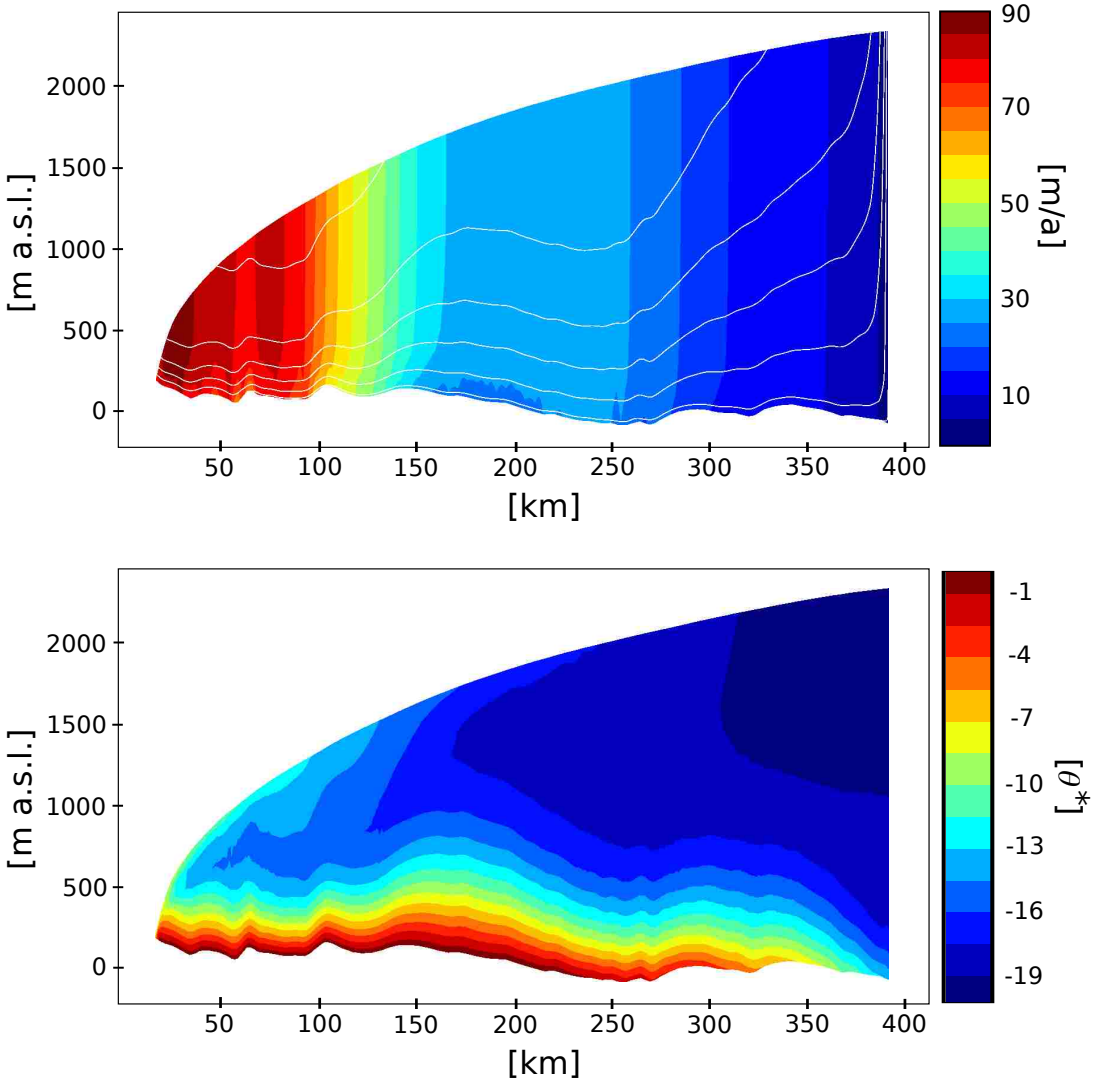

Figure 3.3: The velocity (top) and temperature (bottom) fields produced by the data assimilation process. White lines on the velocity figure indicate flowlines within the velocity field

function in terms of difference between the observed, $u^{\text{obs}}(\mathbf{x})$, and modeled, $u^{\text{mod}}(\mathbf{x})$ surface velocities,

$$g(u,p) = \sum_{i=1}^{N} (u^{\text{obs}}(\mathbf{x_i}) - u^{\text{mod}}(\mathbf{x_i}))^2 \tag{3.20}$$

which will be differentiated with respect to a parameter p that we vary in order to minimize the objective function. In this case the parameter will be $p = \beta(x)^2$ or the basal traction. Our introduction follows that of Strang (2007, pages 678-684).

'Chain rule' differentiation yields

$$\frac{dg}{dp} = \frac{\partial g}{\partial u}\frac{\partial u}{\partial p} + \frac{\partial g}{\partial p}, \tag{3.21}$$

where u is a solution vector containing both velocities and temperatures. The key to efficient calculation of the derivatives of the objective function is writing

$$\frac{\partial g}{\partial u} = c^T \tag{3.22}$$

or, recognizing that the objective function is linear in u. It is now possible to write the gradient as

$$\frac{dg}{dp} = c^T \frac{\partial u}{\partial p} + \frac{\partial g}{\partial p} = c^T A^{-1} \frac{\partial b}{\partial p} + \frac{\partial g}{\partial p}, \tag{3.23}$$

where that $c^T A^{-1}$ is the result of solving the "adjoint" linear system $A^T\lambda = c$ for $\lambda^T = c^T A^{-1}$. Note that the original problem is assumed to be represented by the system of linear equations $Au = b$. Hence, the gradient for each step of an optimization algorithm (we use quasi-Newton) requires a single extra linear solve, rather than a linear solve for each of the many parameters, p. This savings makes it possible to do large inverse problems, such as computing a basal traction for each point in the model domain (see Fig. 2). Figure 3 then corresponds to the initialized velocity and temperature field, or the steady state solutions to the field equations that assimilate the data. This will provide the starting point for all numerical experiments. In some cases, such as determination of the sensitivity to q_g, the entire assimilation/initialization process is repeated with different values.

3.4 Numerical experiments

3.4.1 Sensitivity of the FMB to basal heat flow

In order to determine the sensitivity of the location of the FMB to different values of geothermal heat flux, we performed the data assimilation procedure over a range of possible values. This

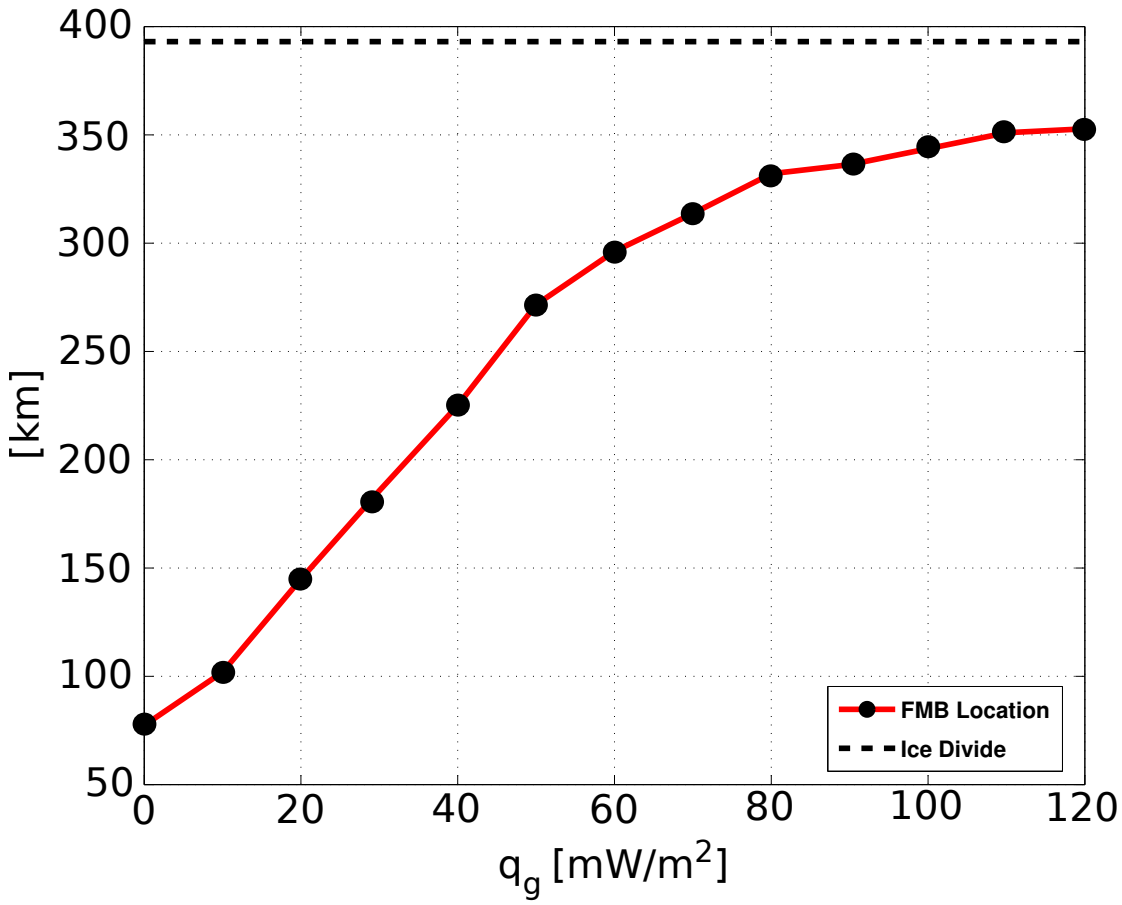

Figure 3.4: Sensitivity of FMB location to variations in the geothermal heat flux.

experiment is motivated by the observation that basal sliding represents a significant portion of the total modelled surface velocity, and we wished to determine the geothermal heat flux required to produce a completely melted bed, in line with the assumption that the bed must be at the melting point for sliding to occur. We conducted model runs at every 5mW/m^{2}within the range 0-120mW/m^2. Figure 3.4 shows the location of the FMB as a function of the prescribed geothermal heat flux. The FMB asymptotically approaches the divide as geothermal heat flux is increased, although the entire bed is not at the melting point under any of the parameter values considered, even for fluxes which seem unreasonably high. For comparison, previous authors have used a value of 42mW/m^2(Pattyn, 2003), and a structural similarity model by Shapiro and Ritzwoller (2004) indicates a mean geothermal heat flux of around 58mW/m^{2}along our flowline.

3.4.2 Sensitivity of the FMB to sliding

Previous work suggests that seasonal changes in the glacial drainage system below the ELA can contribute to changes in basal traction, leading to changes in surface velocity (van de Wal et al., 2008; Bartholomew et al., 2010; Joughin et al., 2008; Zwally et al., 2002). There is little agreement between these papers regarding the magnitude of proposed changes in surface

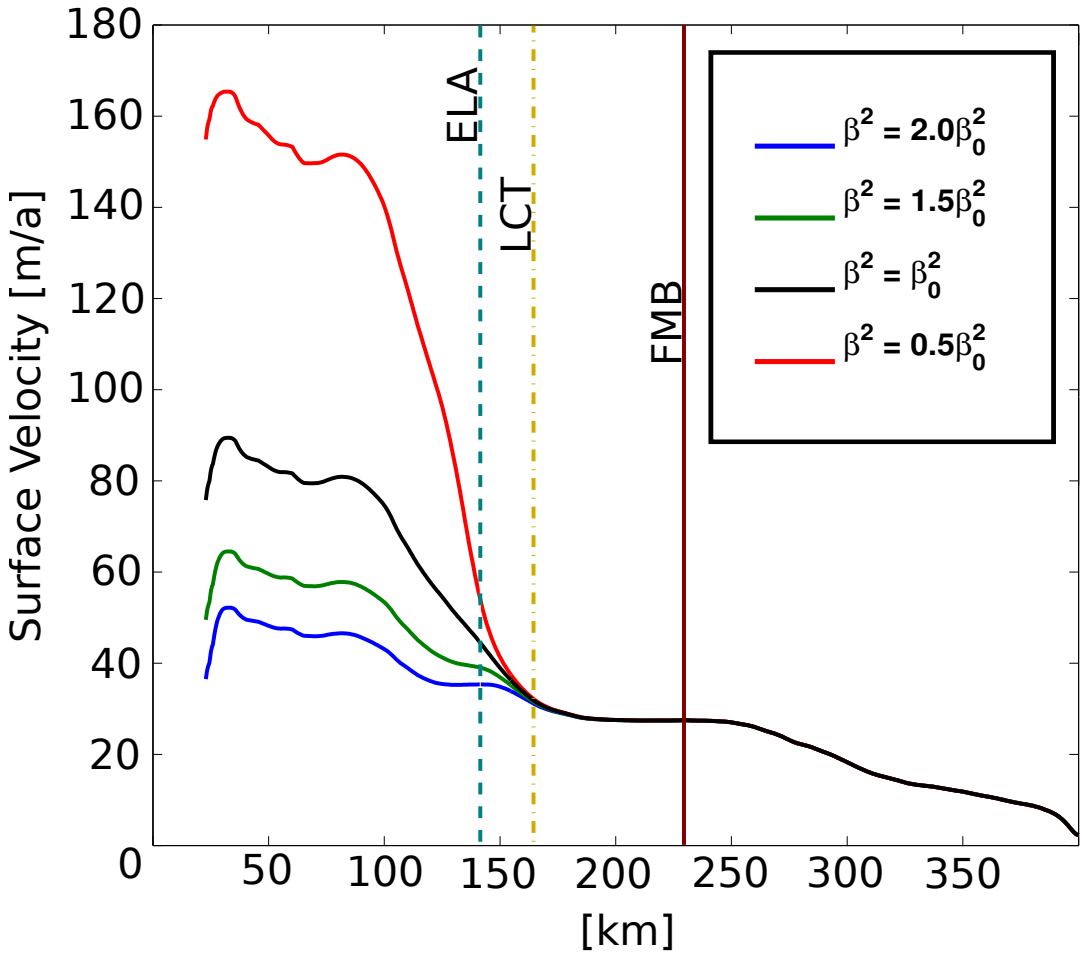

Figure 3.5: Sensitivity of surface velocity to perturbations to the basal traction field, β^2. Equilibrium line altitude (ELA) is approximately 1500ma.s.l. We interpret the longitudinal coupling threshold (LCT) to be the location at which the difference between any two surface velocity profiles is $\leq$1 m/a.

velocity. Joughin et al. (2008) suggests that terrestrially terminating glaciers in the region south of Jakobshavn Isbrae (of which Isunnguata Sermia is one) experience 25% increases in surface velocity as a result of surface melt water lubricating the bed. Bartholomew et al. (2010) suggest speed-ups as great as 200%, and that a warming climate and associated surface lowering will expose greater portions of the bed to surface melt water, increasing the fraction of the ice sheet exposed to summer speed-ups. van de Wal et al. (2008) acknowledge these seasonal variations, but present data which show an overall 10% decrease in surface velocities between 1990 and 2007. They also note that surface ablation and velocity show no correlation.

Regardless of the magnitude and sign of such changes in surface velocity, we sought to determine whether perturbations to the basal traction field, β^2, downstream from the ELA, such as those which would be induced by increased surface meltwater production, would have an impact on the basal thermal regime, specifically the location of the frozen melted boundary. We tested this by inflicting constant multiplicative perturbations to β^2 downstream from the ELA,

ranging between 50% and 200% of the value produced by the data assimilation process. The location of the FMB was insensitive to all of these perturbations. The reason for this is shown in Figure 3.5. Noteable changes in the surface velocity ($>1 \mathrm{ma}^{-1}$) field extend only 20km, or around 10 ice thickness, upstream from the extent of the perturbation. Thus, the advection of heat away from the bed, the dominant mechanism accounting for heat flux at the bed as shown in Figure 3.6, is unchanged 90km upstream, at the location of the FMB. This short coupling distance within the velocity field is corroborated by other studies (Bartholomew et al., 2010; Price et al., 2008).

3.4.3 Heat budget

In order to track the dominant factors which dictate the thermal regime at the bed, we calculated a heat budget of sources and sinks in terms of flux to the ice sheet base. We performed this calculation for a model scenario with optimized β^2 and a geothermal heat flux of $42 \mathrm{mW/m}^2$; results are displayed in Figure 3.6. Upstream of the FMB, frozen conditions are controlled by the advection of cold ice. Near the divide, this advection is predominantly vertically directed from the surface. Moving downstream, advection becomes bed-parallel, so that advective flux decreases to zero at the FMB as heat sources raise the ice temperature as it flows along the bed. Throughout the frozen zone, and some kilometers beyond the FMB, the primary source of heat along the bed is geothermal heat flux. We find that heat generation due to straining at the bed is a positive contributor but negligible compared to geothermal and frictional sources. Downstream of the FMB, excess heat generation is accommodated by the consumption of latent heat associated with the phase transition from ice to water as basal melt occurs. Basal melting initiates at the FMB and steadily increases to a maximum of nearly 20 mm a^{-1} near the terminus.

3.5 Discussion

The sensitivity experiments described above indicate strongly different responses by the FMB to perturbations in geothermal heat flux and basal sliding. The direct response of the basal thermal regime to changes in geothermal heat flux is an expected result. However the diminishing sensitivity of the FMB to increasingly higher heat fluxes is worth noting, and likely reflects the inability of the added heat to overcome cold advected from upstream.

In contrast, longitudinal coupling effects from sliding perturbations below the ELA do not propagate far enough up-glacier to influence the FMB. The location of the FMB is consequently insensitive to such perturbations. This interpretation hinges on the assumption that sliding perturbations apply only below the ELA which is reasonable considering that the effect of increased

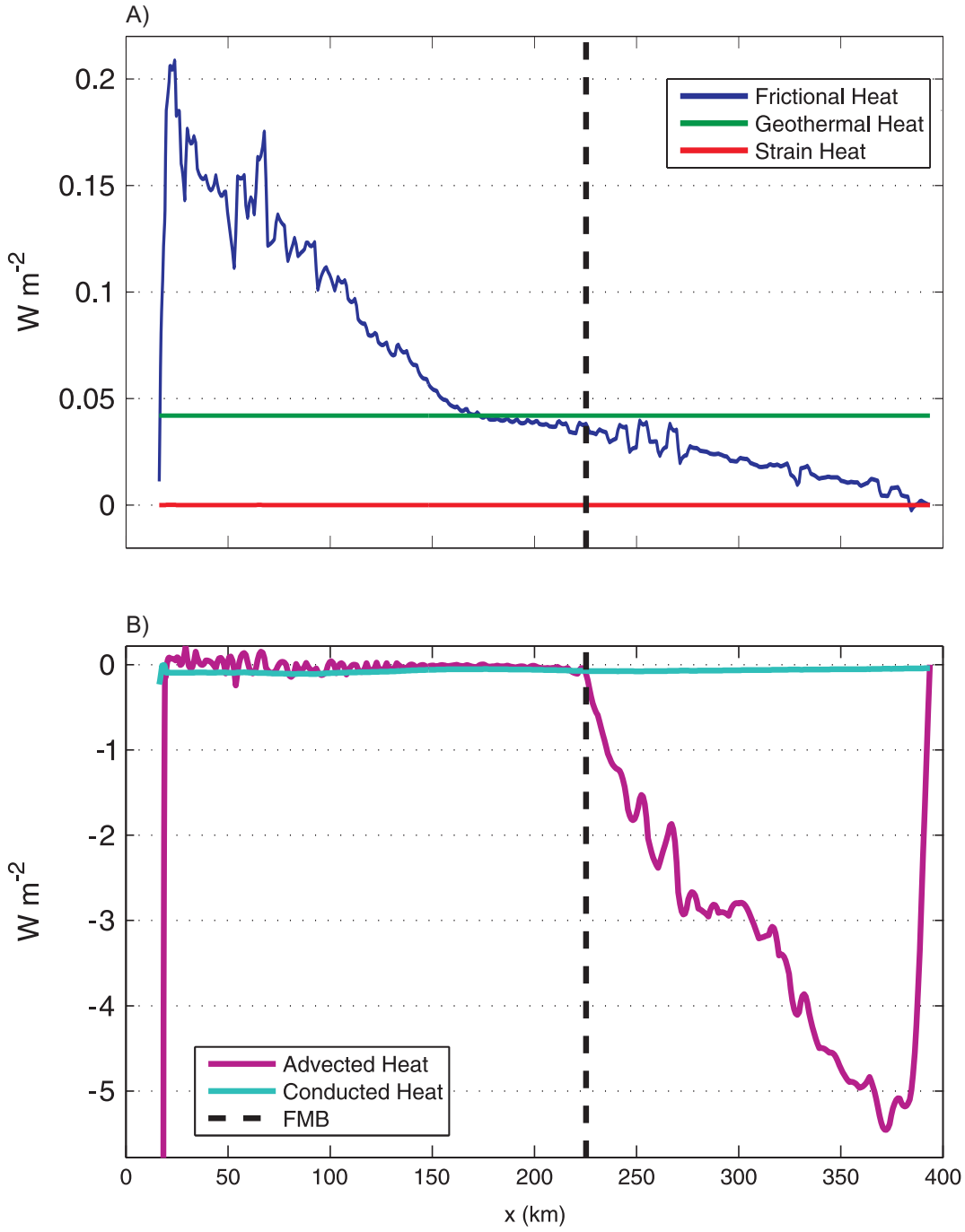

Figure 3.6: Budget of heat sources (A) and sinks (B) along the profile basal boundary. Latent heat generation (not shown here), is a negative non-zero term below the FMB, and accommodates excess heat generated from (A). Strain heat is a positive non-zero term, but negligible compared to frictional and geothermal heat sources.

surface melt input to the basal hydrologic system is not likely to propagate a significant distance upstream along the bed. We hypothesize that the limited distance over which longitudinal coupling occurs is a result of stress being dissipated at the basal boundary. It is important to note that sliding in our model is not limited to below the ELA. In fact, our optimization scheme produces a β^2 field with sliding above the FMB to the ice divide, albeit the upstream sliding is small relative to that occurring near the margin. Migration of melted conditions to the divide does not occur under very high values of geothermal heat flux, thus the representation of sliding in our modeled frozen zone begs explanation.

If the bed is in fact frozen we see several potential explanations for our modeled sliding. First, sliding has been observed over a frozen bed consisting of a till layer (Engelhardt and Kamb, 1998), or hard bedrock (Echelmeyer and Wang, 1987; Cuffey et al., 1999). Additionally, substantial deformation has been observed within a frozen till layer, both within the body of the till itself, (Echelmeyer and Wang, 1987; Engelhardt and Kamb, 1998), as well as along discrete shear planes (Echelmeyer and Wang, 1987). This mechanism may be taking place if such a layer exists beneath GrIS. Second, and perhaps more likely, our model could under-represent velocity from ice deformation, requiring our optimization scheme to over-represent sliding to maintain the observed surface velocity. Changes in flow due to variable impurity and water content and grain size of ice are not accounted for in our model, however elsewhere in Greenland a layer of soft pre-Holocene ice has been observed to enhance flows by 1.7-3.5 fold (Paterson, 1994; Luthi et al., 2002). Alternatively, but in the same vein, the standard constitutive law we use could under-represent grain-scale ice deformation processes (Goldsby and Kohlstedt, 2001). Finally, the velocity field itself could potentially depict a velocity field out-of-balance with the current ice sheet geometry. We have no basis to eliminate any of these possibilities. However, if the magnitude of sliding over frozen bed computed here is not real, it is likely to be principally accounted for by spatial changes in geothermal heat flux, anisotropies within the ice, or a combination of the two.

An alternative scenario is therefore a partitioning of the observed surface velocity with enhanced ice deformation and reduced sliding velocity. Our heat budget along the basal boundary suggests the implementation of sliding has a significant influence on the location of the FMB by increasing the advection of cold ice along the bed. Under this alternative scenario, the associated drop in sliding velocity combined with additional interior heat generation from enhanced straining may modulate the cold contribution from advection, pushing the FMB further upstream. These processes would likely be countered by a decrease in frictional heating, which would force the FMB towards the margin. A model exploration of FMB migration from this interaction of heat sources is beyond the scope of this manuscript, and will be the focus of future work.

3.6 Conclusion

We developed a thermomechanically coupled, 2-dimensional flowline model, which was applied to a terrestrially terminating glacier profile located in western Greenland. We extracted geometric information for the model domain from a dataset presented in Bamber et al. (2001), which we believe to be the best data available at present for the Greenland Ice Sheet. We used adjoint methods to optimize the basal traction field, such that modelled surface velocities matched observed values (Joughin et al., 2010) to within $1\mathrm{ma}^{-1}$.

With an optimized model in hand, we conducted experiments in order to determine the sensitivity of the frozen-melted boundary (FMB) to perturbations in the basal heat flux and basal traction downstream of the ELA. We found that the FMB migrates easily under different assumptions about geothermal heat flux. At values close to $0\mathrm{mW/m}^2$, the FMB moves very close to the terminus, but part of the bed remains unfrozen due to frictional heating from sliding. At high values, the FMB asymptotically approaches the ice divide. We found that for reasonable perturbations to basal traction downstream from the ELA, such as what might be expected from an increase in surface meltwater production and associated bed lubrication, the FMB was insensitive. This is a result of the short length scale over which longitudinal stress coupling in the ice operates ($\sim$10 ice thicknesses). The FMB is significantly further upstream from the ELA than the perturbations to the velocity field extend, thus advective heat fluxes are unchanged. Our model predicts that under most assumptions about geothermal heat flux, sliding occurs over a frozen bed. We see two possible explanations for this: 1) That this sliding is real, and follows one of the mechanisms proposed by Echelmeyer and Wang (1987), Engelhardt and Kamb (1998), or Cuffey et al. (1999), 2) Anisotropies or variability in hardness within the ice result in a preferential flow direction and increased deformation. Additional work is needed to quantify the sensitivity of the basal thermal regime to the second of these factors.

Future work

The three previous chapters documented both the theory behind and applications of a state of the art ice sheet model. I argue that the use of a variational principle as the starting point for modelling the ice momentum balance is a fundamentally better way to approach ice sheet modelling. The same is true of the enthalpy formulation compared to previous methods for solving the energy balance. The coupling of these two methods is another advancement in its own right. Performing inversions on the first order model is fairly new and the level of success in inversion is notable. The use of finite elements as a modelling framework is an advancement over the classical ice sheet model approach of finite differences.

Despite these advances, there a number of ways that the model needs to be improved, as well as additional scientific work that could capitalize on the developments presented herein.

First and perhaps most importantly, the dynamic component of the model needs to be improved. As it stands, the methods of updating model geometry are crude, and depend on solving a fundamentally unstable equation. Some of the particular free surface challenges associated with ice, such as the capacity for ice to override itself, are made explicitly impossible given the current method of time stepping. Approaching the problem from a Lagrangian (moving frame of reference) versus Eulerian (fixed frame) perspective may be a way to overcome these problems. A starting point to this approach is given by Dukowicz and Baumgardner (2000).

Second, the model must be expanded to three spatial dimensions. The flowline model is efficient and can provide insight into a number of glaciological problems, but it neglects transverse effects and is highly limited in terms of its spatial applicability. The way to proceed is to parameterize the spatial dimensions of the model, such that the physics can be applied in any number and any combination of dimensions.

Third, a Tikhonov regularization term should be applied to the optimization routine. As it stands, the model is not penalized for overfitting the basal traction field, and oscillatory solutions are the result. A penalty function on the second derivative of β^2 would help to correct this. Intuitively, this means adding some stiffness to the line that defines the basal traction field. If performing the unregularized inversion is akin to laying out a string such that the string forms

a plot of the optimal values of β^2, the regularized inversion is like using a wire. This would lend confidence to actually drawing conclusions from the structure of the field itself.

Finally, the model should be applied to more glaciological problems. There are a number of questions that it could help address. How stable is the current configuration of the ice sheet, given modern temperature and mass balance? How well do the current data sets for bed and surface elevation conserve mass, under the assumption of a steady state ice sheet? What are the effects of short scale changes in the basal traction field due to influxes of summer surface meltwater? Does assuming different rheologic properties at different age layers affect the velocity structure of the ice sheet? The model presented herein is well-equipped to answer any of these.

Bibliography

Andersen, K. K. et al. (2004). High-resolution record of northern hemisphere climate extending into the last interglacial period. *Nature*, 431:147–151.

Aschwanden, A. and Blatter, H. (2009). Mathematical modeling and numerical simulation of polythermal glaciers. *Journal of Geophysical Research*, 114.

Bamber, J. L., Layberry, R. L., and Gogineni, S. P. (2001). A new ice thickness and bed data set for the greenland ice sheet 1. measurement, data reduction, and errors. *J. Geophys. Res.*, 106(D24):33773–33780.

Bartholomew, I., Nienow, P., Mair, D., Hubbard, A., King, M. A., and Sole, A. (2010). Seasonal evolution of subglacial drainage and acceleration in a greenland outlet glacier. *Nature Geosci*, advance online publication.

Blatter, H. (1995). Velocity and stress fields in grounded glaciers: A simple algorithm for including deviatoric stress gradients. *Journal of Glaciology*, 41:331–344.

Chandler, D. M., Hubbard, A. L., Hubbard, B. P., and Nienow, P. W. (2006). A monte carlo error analysis for basal sliding velocity calculations. *J. Geophys. Res.*, 111(F4):F04005.

Cuffey, K. M., Conway, H., Hallet, B., Gades, A. M., and Raymond, C. F. (1999). Interfacial water in polar glaciers and glacier sliding at 17°C. *Geophys. Res. Lett.*, 26(6):751–754.

Dahl-Jensen, D., Mosegaard, K., Gundestrup, N., Clow, G. D., Johnsen, S. J., Hansen, A. W., and Balling, N. (1998). Past temperatures directly from the greenland ice sheet. *Science*, 282(5387):268–271.

Davis, T. (2004). A column pre-ordering strategy for the unsymmetric-pattern multifrontal method. *AMS Trans. Math. Software*, 30:165–195.

Deuflhard, P. (1974). A modified newton method for the solution of ill-conditioned systems of nonlinear equations with application to multiple shooting. *Numer. Math*, 22:289–315.

Dukowicz, J. and Baumgardner, J. R. (2000). Incremental remapping as a transport/advection algorithm. *J. Comput. Phys.*, 160:318–335.

Dukowicz, J. K. (2011). Reformulating the full-stokes ice sheet model for a more efficient computational solution. *The Cryosphere Discussions*, 5(4):1749–1774.

Echelmeyer, K. and Wang, Z. (1987). Direct observation of basal sliding and deformation of basal drift at sub-freezing temperatures. *Journal of Glaciology*, 33(113).

Engelhardt, H. and Kamb, B. (1998). Basal sliding of ice stream b, west antarctica. *Journal of Glaciology*, 44(147).

Ettema, J., van den Broeke, M. R., van Meijgaard, E., van de Berg, W. J., Bamber, J. L., Box, J. E., and Bales, R. C. (2009). Higher surface mass balance of the greenland ice sheet revealed by high-resolution climate modeling. *Geophys. Res. Lett.*, 36(12):L12501.

Fahnestock, M., Adbalati, W., Joughin, I., Brozena, J., and Gogineni, P. (2001). High geothermal heat flow, basal melt, and the orgin of rapid ice flow in central greenland. *Science*, 294:2338–2342.

Flowers, G. E., Björnsson, H., and Pàlsson, F. (2002). New insights into the subglacial and periglacial hydrology of vatnajökull, iceland, from a distributed physical model. *Journal of Glaciology*, 48:467–477.

Glen, J. W. (1955). The creep of polycrystalline ice. *Proceedings of the Royal Society, A*, 228:519–538.

Goldberg, D. N. and Sergienko, O. V. (2011). Data assimilation using a hybrid ice flow model. *The Cryosphere*, 5(2):315–327.

Goldsby, D. L. and Kohlstedt, D. L. (2001). Superplastic deformation of ice: Experimental observations. *J. Geophys. Res.*, 106(B6):11017–11030.

Greve, R. (2005). Relation of measured basal temperatures and the spatial distribution of the geothermal heat flux for the greenland ice sheet. *Annals of Glaciology*, 42:424–432(9).

Greve, R. and Hutter, K. (1995). Polythermal three-dimensional modelling of the greenland ice sheet with varied geothermal heat flux. *Annals of Glaciology*, 21:8–12.

Gudmundsson, G. H. and Raymond, M. (2008). On the limit to resolution and information on basal properties obtainable from surface data on ice streams. *The Cryosphere*, 2(2):167–178.

Guymon, G. L., Scott, V. H., and Herrmann, L. R. (1970). A general numerical solution of the Two-Dimensional Diffusion-Convection equation by the finite element method. *Water Resour. Res.*, 6(6):1611–1617.

Heimbach, P. and Bugnion, V. (2009). Greenland ice-sheet volume sensitivity to basal, surface and initial conditions derived from an adjoint model. *Annals of Glaciology*, 50(52).

Hindmarsh, R. C. A. (2004). A numerical comparison of approximations to the stokes equations used in ice sheet and glacier modeling. *J. Geophys. Res*, 109(F01012):doi:10.1029/2003JF000065.

Hughes, J. R. (2000). *The Finite Element Method, Linear Static and Dynamic Finite Element Analysis*.

Hutter, K. (1982). A mathematical model of polythermal glaciers and ice sheets. *Geophysical and Astrophysical Fluid Dynamics*, 21(3-4):201–224.

Huybrechts, P., Payne, T., Abe-Ouchi, A., Calov, R., Fastook, J., Greve, R., Hindmarsh, R., Hoydal, O., Johannesson, T., MacAyeal, D., Marsiat, I., Ritz, C., Verbitsky, M., Waddington, E., and Warner, R. (1996). The eismint benchmarks for testing ice-sheet models.

Joughin, I., Das, S. B., King, M. A., Smith, B. E., Howat, I. M., and Moon, T. (2008). Seasonal Speedup Along the Western Flank of the Greenland Ice Sheet. *Science*, 320(5877):781–783.

Joughin, I., Smith, B. E., Howat, I. M., Scambos, T., and Moon, T. (2010). Greenland flow variability from ice-sheet-wide velocity mapping. *Journal of Glaciology*, 56(197).

Larour, E., Rignot, E., Joughin, I., and Aubry, D. (2005). Rheology of the ronne ice shelf, antarctica, inferred from satellite radar interferometry data using an inverse control method. *Geophys. Res. Lett.*, 32(5):L05503.

Logg, A. and Wells, G. N. (2010). Dolfin: Automated finite element computing. *ACM Trans. Math. Softw.*, 37:20:1–20:28.

Luthi, M., Funk, M., Iken, A., Gogineni, S. P., and Truffer, M. (2002). Mechanism of fast flow in jakobshavns isbrae, west greenland. part iii. measurements of ice deformation, temperature and cross-borehole conductivity in boreholes to the bedrock. *Journal of Glaciology*, 48(162):369–385.

MacAyeal, D. R. (1993). A tutorial on the use of control methods in ice-sheet modeling. *J. Glaciol.*, 39(131):91–98.

MacAyeal, D. R., Rommelaere, V., Huybrechts, P., Hulbe, C. L., Determann, J., and Ritz, C. (1996). An ice-shelf model test based on the ross ice shelf, antarctica. *Annals of Glaciology*, 23:46–51.

Morlighem, M., Rignot, E., Seroussi, H., Larour, E., Dhia, H. B., and Aubry, D. (2010). Spatial patterns of basal drag inferred using control methods from a full-stokes and simpler models for pine island glacier, west antarctica. *Geophysical Research Letters*, 37.

Nocedal, J. and Wright, S. (2006). *Numerical Optimization*. Springer, 2 edition.

Nowicki, S. and Wingham, D. (2008). Conditions for a steady ice sheetice shelf junction. *Earth and Planetary Science Letters*, 265(1-2):246 – 255.

Oswald, G. K. A. and Gogineni, S. P. (January 2008). Recovery of subglacial water extent from greenland radar survey data. *Journal of Glaciology*, 54:94–106(13).

Paterson, W. and Budd, W. (1982). Flow parameters for ice sheet modeling. *Cold Regions Science and Technology*, 6(2):175–177.

Paterson, W. S. B. (1994). *The Physics of Glaciers*.

Pattyn, F. (2003). A new three-dimensional higher-order thermomechanical ice-sheet model: basic sensitivity, ice-stream development and ice flow across subglacial lakes. *Journal of Geophysical Research (Solid Earth)*, 108(B8):2382.

Pattyn, F., Perichon, L., Aschwanden, A., Breuer, B., de Smedt, B., Gagliardini, O., Gudmundsson, G. H., Hindmarsh, R. C. A., Hubbard, A., Johnson, J. V., Kleiner, T., Konovalov, Y., Martin, C., Payne, A. J., Pollard, D., Price, S., Rückamp, M., Saito, F., Souček, O., Sugiyama, S., and Zwinger, T. (2008). Benchmark experiments for higher-order and full-stokes ice sheet models (ismiphom). *The Cryosphere*, 2(2):95–108.

Price, S. F., Payne, A. J., Catania, G. A., and Neumann, T. A. (2008). Seasonal acceleration of inland ice via longitudinal coupling to marginal ice. *Journal of Glaciology*, 54(185):213–219.

Rutt, I. C., Hagdorn, M., Hulton, N. R. J., and Payne, A. J. (2009). The glimmer community ice sheet model. *J. Geophys. Res.*, 114(F2):F02004.

Schäfer, M., Gagliardini, O., Pattyn, F., and Le Meur, E. (2008). Applicability of the shallow ice approximation inferred from model inter-comparison using various glacier geometries. *The Cryosphere Discussions*, 2(4):557–599.

Schoolf, C. and Hindmarsh, R. (2010). Thin-film flows with wall slip: an asymptotic analysis of higher order glacier flow models. *Quarterly Journal of Applied Mathematics*, 63(1):73–114.

Shapiro, N. M. and Ritzwoller, M. H. (2004). Inferring surface heat distributions guided by global seismic model: particular applications to antarctica. *Earth Planet. Sci. Lett.*, 223:69–84.

Strang, G. (2007). *Computation Science and Engineering*.

Vainberg, M. M. (1964). *Variational Methods for the Study of Nonlinear Operators*. Holden-Day, San Fransisco.

van de Wal, R. S. W., Boot, W., van den Broeke, M. R., Smeets, C. J. P. P., Reimer, C. H., Donker, J. J. A., and Oerlemans, J. (2008). Large and rapid melt-induced velocity changes in the ablation zone of the greenland ice sheet. *Science*, 321:111–113.

Weertman, J. (1968). Comparison between measured and theoretical temperature profiles of the camp century, greenland, borehole. Technical Report 246.

Weis, M., Greve, R., and Hutter, K. (1999). Theory of shallow ice shelves. *Continuum Mechanics and Thermodynamics*, 11:15–50.

Zienkiewicz, O. C. and Taylor, R. L. (2000). *The Finite Element Method*. Butterworth-Heinemann, Oxford, 5 edition.

Zwally, H. J., Abdalati, W., Herring, T., Larson, K., Saba, J., and Steffen, K. (2002). Surface melt- induced acceleration of greenland ice-sheet flow. *Science*, 297:218–222.